

# Continental-scale prediction of hydrologic signatures and processes

Ryoko Araki<sup>1,2</sup>, Anne Holt<sup>1</sup>, John C. Hammond<sup>3</sup>, Admin Husic<sup>4</sup>, Gemma Coxon<sup>5</sup>, Hilary K. McMillan<sup>1</sup>

<sup>1</sup>Department of Geography, San Diego State University, San Diego, CA, USA.

<sup>2</sup>Department of Geography, University of California, Santa Barbara, Santa Barbara, CA, USA.

<sup>3</sup>U.S. Geological Survey, Maryland–Delaware–DC Water Science Center, Baltimore, MD, USA.

<sup>4</sup>Department of Civil and Environmental Engineering, Virginia Tech, Blacksburg, VA, USA.

<sup>5</sup>School of Geographical Sciences, University of Bristol, Bristol, UK.

*Correspondence to:* Ryoko Araki (raraki8159@sdsu.edu; raraki@ucsb.edu) and Hilary McMillan (hmcmillan@sdsu.edu)

**Abstract.** Understanding how dominant hydrologic processes and their drivers vary across diverse continental-scale landscapes is critical for hydrologic modeling and water management applications. Our research addresses this question by synthesizing large-sample watershed datasets, Caravan and GAGES-II, and developing random forest models to identify patterns in hydrologic [behavior/function](#). We assessed dominant processes by examining hydrologic signatures—summary indicators of watershed [behavior-function](#) derived from hydroclimatic time series and random forest models across 14,146 gauged U.S. watersheds. The results reveal clear continental-scale gradients in hydrologic processes, including baseflow, overland flow, storage, and water balance losses. Our map of dominant processes highlights, for example, the transition from baseflow to fast responses and back to baseflow along the elevation gradient from the Appalachian spine, through the Piedmont, to the Eastern Coastal Plain; a distinct outer ring around the Great Lakes region; and sharp contrasts between coastal and inland processes in the West. Variable importance analysis from random forest models show that processes in the western U.S. are primarily controlled by climate, whereas in the eastern U.S., soil, geology, and topography play larger roles, with distinct human influences apparent in urban areas. Our [approach of estimates-estimating of](#) dominant processes and their drivers [provide a framework to-facilitates](#) extending process knowledge from research watersheds to the continental scale, [assessing](#) current hydrological understanding, and [evaluating](#) hydrological model structures.

## 1 Introduction

### 1.1 Identifying hydrologic processes at large scales

Estimating the contributions of different hydrologic processes to streamflow generation at a continental scale is essential for flood forecasting and water resources management. Optimal management strategies, including the design of grey and green infrastructure, differ depending on which processes dominate hydrological response (Oswald et al., 2023; Thompson et al., 2020), which vary substantially by regional environmental conditions (Blöschl, 2006; Paola et al., 2006; Penna, 2024). Understanding how water is partitioned, stored, and transported through different parts of the terrestrial systems is a fundamental question in the hydrologic sciences (Brooks et al., 2015). To simulate a diverse set of processes at large-scale, a new generation of hydrologic models with flexible and heterogeneous structures has emerged (Clark et al., 2015; Frame et al., 2025; Johnson et al., 2023). However, despite these technological advances, we still lack an estimate of dominant hydrologic

34 processes controlling streamflow generation at continental scales (McMillan et al., 2025; Reinecke et al., 2025). Developing  
35 this understanding is a critical step toward unified hydrologic theory (Sivapalan, 2005) and can provide a blueprint for robust  
36 model development and informed decision making.

37  
38 Previous efforts to map multiple hydrologic processes at continental scales are scarce. ~~Instead, studies at Most large-scale~~  
39 ~~studies~~ have typically focused on ~~one-one~~ process, while others have studied multiple processes for single or small groups of  
40 watersheds. For example, Buchanan et al., 2018. ~~Examples include studies that examined/assessed~~ the likelihood of infiltration  
41 excess flow occurrence by comparing whether rainfall intensity exceeds saturated hydraulic conductivity, ~~finding that~~  
42 ~~saturation excess dominates across the contiguous U.S., while infiltration excess is regionally likely in the central U.S.~~  
43 ~~(Buchanan et al., 2018); Similarly, studies on~~ baseflow indices ~~have shown their strong dependence on climatic and soil~~  
44 ~~properties and their drivers globally~~ (Beck et al., 2013; Xie et al., 2024), and Fang and Shen (2017) quantified the ~~strength~~  
45 ~~of~~ runoff-storage connectivity ~~through using a~~ correlations between anomalies in streamflow gauge and satellite water storage  
46 observations, ~~highlighting large-scale interactions among groundwater table, soil thickness, topography, and snow.~~ (Fang and  
47 ~~Shen, 2017); In contrast, studies that examined multiple processes have been typically focused on a single or small groups of~~  
48 ~~watersheds.~~ A study in Alaska shows that the use of multiple streamflow statistics can help distinguish and assign hydrologic  
49 regions (Barnhart et al., 2022). Model-aided studies have simulated global patterns of multiple indices: water partitioning into  
50 green and blue water, streamflow response elasticity to rainfall, and streamflow flashiness (Ji et al., 2025), U.S.-wide indices  
51 for water balance seasonality (Berghuijs et al., 2014). Another model-based approach has involved inferring hydrologic  
52 processes through parameter sensitivity analysis (Hay et al., 2023). These synthesis studies present promising descriptions of  
53 spatial patterns and directions for future progress toward a holistic understanding of runoff generation mechanisms, which still  
54 remains elusive.

55  
56 Much of the research for generalizing watershed ~~behaviors-function~~ has focused on summarizing flow regimes (Dettinger and  
57 Diaz, 2000; Lane et al., 2017; Lee et al., 2015; Lins, 1997) and predicting shifts in flow regime under future climate (Brunner  
58 et al., 2020; Hodgkins et al., 2024). Many studies cluster streamflow gauges using flow indices, ~~that target-targeting~~ general  
59 (Almagro et al., 2024; Ariano and Ali, 2025; Mosley, 1981; Wu et al., 2021), intermittent (Sauquet et al., 2021), or seasonal  
60 streamflow patterns (Dhungel et al., 2016; Haines et al., 1988; Kennard et al., 2010). However, most of these studies aim to  
61 define the similarity of flow regimes rather than the underlying runoff generation processes. Furthermore, the results from  
62 clustering approaches are constrained to gauged locations and lack spatial coherence, making it challenging to extrapolate to  
63 ungauged watersheds.

64  
65 To estimate watershed processes in ungauged locations, hydrologists have conventionally used maps derived from  
66 physiographic datasets. For example, in the United States context, the Environmental Protection Agency's Ecoregions  
67 (Omernik, 1987, 2004), an ecosystem classification based on the physical and biotic characteristics, is a common reference

68 when discussing hydrologic processes (Falcone et al., 2010). Other classifications include the United States Geological  
69 Survey's Water Resources Regions (Seaber et al., 1987) based on streamflow networks, Hydrologic Landscape Regions  
70 (Santhi et al., 2008; Winter, 2001; Wolock, 2003a) based on physiographic and climatic datasets, and the United States  
71 Department of Agriculture's Hydrologic Soil Groups (Web Soil Survey, 2025) based on soil surveys. Nevertheless,  
72 regionalization based on physiographic data often fails to capture the full variability of watershed [behavior-function](#) (Ali et al.,  
73 2012; Oudin et al., 2008) because hydrologic processes can differ even among physiographically similar watersheds (McMillan  
74 et al., 2014). Capturing watershed processes at a continental scale calls for a scalable method to draw information from  
75 hydroclimatic datasets. To date, no studies have attempted to develop comprehensive maps of runoff generation processes  
76 based on streamflow observations that can effectively capture watersheds' functions.

## 77 1.2 Hydrologic signatures links to processes

78 Hydrologic signatures are metrics that quantify hydrologically-relevant dynamics, and offer a promising way to infer watershed  
79 processes with minimal data requirements (McMillan, 2021). Hydrologic signature calculations require only widely-available  
80 datasets, such as streamflow and precipitation, and can be related to various watershed processes, such as runoff generation  
81 and water storage dynamics (McMillan, 2020; Wlostowski et al., 2021). Using hydrologic signatures, expert knowledge, and  
82 landscape characteristics, Fenicia and McDonnell (2022) inferred dominant runoff processes and developed perceptual models  
83 at the regional scale; and Pechlivanidis and Arheimer (2015) mapped process differences at the national scale in India.  
84 Hydrologic signatures can capture the functional streamflow responses to climatic forcings and can discriminate different  
85 processes across landscapes (Araki et al., 2022; Gnann et al., 2020, 2021a; Janssen and Ameli, 2021). This enables a signature-  
86 based exploration of the relationship between landscape form and function (Bracken et al., 2013; Sivapalan, 2005).

## 87 1.3 Predicting hydrologic signatures using watershed attributes

88 Watershed attributes describe the physical characteristics of watersheds, which can be used to identify the drivers of hydrologic  
89 processes and to transfer hydrological knowledge to ungauged locations (Tarasova et al., 2023). The link between watershed  
90 attributes and signatures of streamflow response can be explored via machine learning approaches on large watershed samples.  
91 Regional and global applications include studies in the U.S. (Addor et al., 2018; Janssen and Ameli, 2021; Wu et al., 2021),  
92 Australia (Trancoso et al., 2017), Zimbabwe (Mazvimavi et al., 2005), Brazil (Almagro et al., 2024), Europe ([Rudlang et al.,  
93 2025](#); Kuentz et al., 2017), and globally (Beck et al., 2015). Across all studies, climate emerged as the primary control on  
94 signatures. Non-climatic factors (i.e., landscape attributes), such as soil, geology, vegetation cover, and topography, had weak  
95 or limited predictive power. However, substantial evidence from field-based studies shows that landscape forms are a primary  
96 control of watershed function (Angermann et al., 2017; Fan et al., 2019; Jackisch et al., 2017; Jefferson et al., 2010; Lohse and  
97 Dietrich, 2005; Pfister et al., 2017; Zimmer and Gannon, 2018).

98

99 Weak predictive power of non-climatic drivers can be attributed to lack of high-resolution, accurate landscape attributes that  
100 describe regionally important processes (Gnann et al., 2021a; Tarasova et al., 2023). For example, wetlands are key regulators  
101 of low flows in the U.S. (Worland et al., 2018) and have been left out of previous studies (Addor et al., 2018). Similarly,  
102 weathering and glaciation have primary impacts on baseflow storage and generation (Neff et al., 2005; Tague and Grant, 2004),  
103 but rock permeability and porosity predictors did not clearly capture the relationship (Wu et al., 2021). Coarse spatial resolution,  
104 or limited quality and consistency of global datasets may reduce their predictive power (Nascimento et al., 2025; Beck et al.,  
105 2015; Tarasova et al., 2023). ~~Additionally, large-sample studies across broad climatic gradients may be obscuring the~~  
106 ~~influences of landscape attributes.~~ Regional analysis can mitigate ~~eliminate this effect influence~~ and elucidate the ~~contribution~~  
107 ~~of non-climatic drivers; for example, such as~~ regional random forest models ~~that have~~ revealed physiographic and  
108 anthropogenic controls on flow regimes (Almagro et al., 2024; Hammond et al., 2021). However, smaller regional sample  
109 sizes may limit prediction accuracy if datasets only provide tens of watersheds per region (Willard et al., 2024).

110  
111 Lastly, the quality of signatures can compromise data-driven model performance and interpretation for process understanding.  
112 Examples include the sensitivity of flow duration curve slope to measurement errors (McMillan et al., 2017), the sensitivity of  
113 signatures to rating curve uncertainties (Westerberg et al., 2016), lack of process representativeness (McMillan et al., 2022),  
114 and inaccurate parameterization of storm separation algorithms (McMillan et al., 2023). Minimizing the impact of signature  
115 uncertainty is important for differentiating different regional watershed functionalities (Westerberg et al., 2016).

#### 116 **1.4 Aims of the paper**

117 This study presents the first hydrologic processes map for the contiguous United States (CONUS). We synthesized hydrologic  
118 signatures as process indicators, going beyond pattern identification from single signatures. We hypothesize that signature  
119 combinations can represent six key hydrologic processes (McMillan, 2020; McMillan et al., 2022): baseflow and storage,  
120 water balance and seasonal flow variability, and saturation and infiltration excess overland flow. Using random forest models,  
121 we demonstrate the explanatory power of landscape metrics to predict hydrologic signatures and their regional variations, and  
122 thus the underlying processes, across CONUS.

123  
124 We address the limitations of previous studies in predicting hydrologic signatures. First, we improved the quality of non-  
125 climatic attributes by: (i) incorporating new geological and wetland landscape attributes that have demonstrated strong  
126 connections to baseflow processes (Holt and McMillan, 2025); and (ii) utilizing watershed attributes from GAGES-II datasets  
127 (Falcone, 2011), derived from survey-based and higher-resolution products. Second, we interpret random forests using Shapley  
128 values (Shapley, 1953) following Husic et al. (2025), as well as permutation importance values within a regional model-  
129 building approach, following Hammond et al. (2021), which extends prior work to elucidate the regional contributions of non-  
130 climatic, landscape attributes to hydrologic processes. Furthermore, our work assessed 14,146 U.S. watersheds and was trained  
131 on 10,261 watersheds, nearly ten times more sample watersheds than previous studies; we leverage the Caravan and GAGES-

132 II—the most extensive open-source large-sample datasets currently available (Falcone, 2011; Kratzert et al., 2023). Third, we  
133 utilize a set of hydrologic signatures proven robust across large-sample watershed studies and have a clear connection to  
134 critical-zone processes (McMillan et al., 2022), with their parameters further tuned to local storm characteristics. With these  
135 improvements, we expand watershed coverage and uncover more detailed spatial patterns of watershed processes than  
136 previously possible, using widely-available hydroclimatic datasets and physiographic attributes.

## 137 **2 Data**

138 We used two primary sources of streamgages and watershed attribute data to expand the number of samples: Caravan v1.5  
139 (Kratzert et al., 2023, 2024) and U.S. Geological Survey GAGES-II (Falcone, 2011; Falcone et al., 2010). See Fig. 1 for the  
140 spatial distribution of the study watersheds. Caravan is an open-source dataset of global watersheds; its CONUS subset consists  
141 of 9,234 watersheds sourced from CAMELS-US (Addor et al., 2017) and HYSETS (Arsenault et al., 2020). GAGES-II is a  
142 geospatial dataset of 9,067 watersheds in the United States, selected for their quality to characterize natural and altered flow  
143 regimes.

### 144 **2.1 Hydroclimatic dataset**

145 We calculated hydrologic signatures listed in Table 1 using daily hydroclimatic timeseries data from watersheds within the  
146 contiguous United States (CONUS). For Caravan watersheds, we used U.S. Geological Survey (USGS) streamflow  
147 measurements paired with daily ERA5-Land forcings provided. For the GAGES-II watersheds, we obtained the USGS  
148 streamflow records (U.S. Geological Survey, 2025) using the dataRetrieval package (DeCicco et al., 2018) and gridMET  
149 forcings from Wiczorek et al. (2023). For calculating infiltration excess overland flow signatures of Wu et al. (2021;  
150 “*RC\_Pint*”), we used the hourly precipitation from the North American Land Data Assimilation System 2 (NLDAS-2; Xia et  
151 al., 2012) provided through CAMELSH: a Large-Sample Hourly Hydrometeorological Dataset and Attributes at Watershed-  
152 Scale for CONUS (Tran, 2025; Tran et al., 2025).

### 154 **2.2 Watershed attributes**

155 We combined watershed attributes from three sources: (1) Caravan, (2) GAGES-II, and (3) geologic age and wetland attributes  
156 (Holt and McMillan, 2025). We added average geologic age and isolated wetland fraction metrics because of their strong link  
157 to baseflow processes, which were missing from previous large-sample analyses (Holt and McMillan, 2025). From the Caravan  
158 and Holt & McMillan (2025) attribute sets, we excluded binary or categorical attributes, monthly climate variables,  
159 uninformative attributes for the CONUS context (e.g., permafrost extent, gross domestic product), and highly correlated  
160 attributes (Spearman's rho > 0.8 or < -0.8; see Text S1). Where available, Caravan attributes were substituted with GAGES-II  
161 attributes, as described in Section 3.2 and Table S1. Table 2 lists the 23 attributes used in the random forest analysis. [The](#)

162 purpose of merging Caravan and GAGES-II dataset is to maximize the sample size of watersheds and better capture regional  
163 hydrologic variability (see Table S1 and an associated Venn diagram of watershed coverage across datasets).

### 164 **3 Method**

165 We analyzed 14,146 gauged U.S. watersheds; our map of processes was based on observational data from 10,261 gauged sites  
166 and extended using random forest predictions to an additional 3,885 watersheds. See Table S1 and associated figures for an  
167 overview of the datasets used and the workflow.

Formatted: Normal

#### 168 **3.1 Calculating hydrologic signatures**

169 A total of 12 signatures (four baseflow and groundwater signatures, four water balance and seasonality-related signatures, and  
170 four overland flow signatures) were used to characterize hydrologic dynamics (see Table 1). The signatures were selected  
171 based on their reliability in representing processes (McMillan et al., 2022). We calculated signatures using the TOSSH toolbox  
172 (Gnann et al., 2021b) and tuned the parameters for event separation for each hydroclimatic region (see Tables S2, S3).

173 ~~Furthermore, we omitted~~ We filtered out watersheds from our training-signature calculations based on quality criteria for  
174 watershed area and snow used by previous studies, and on the timeseries length needed for signatures to stabilize. First, we  
175 removed watersheds from our analysis with uncertain topographic boundaries, showing high discrepancies (>25%) in the  
176 estimated drainage area between GAGES-II and Caravan datasets. Errors of <20% are possible due to differences in watershed  
177 delineation tools or missing small tributaries (Ray, 2018). Second, for overland flow signature analysis, we excluded snow-  
178 dominated watersheds (>20% snow fraction of total precipitation; a >30% criterion were used in McMillan et al., 2022 and  
179 Wu et al., 2021); this is because our overland flow signatures can be heavily influenced by periods with no flow response due  
180 to snow or frozen conditions. Third, we excluded watersheds with less than 5 years of streamflow observation record, and  
181 those with over 30% missing daily data over the period where streamflow was recorded (yielding at least three years of  
182 available data). Studies suggest that temporal hydrologic variability is adequately captured with 3 to 5 years of data (Refsgaard  
183 and Storm, 1996; Klemeš, 1986; Merz et al., 2009).

#### 185 **3.2 Training random forest models and predicting hydrologic signatures**

186 We developed random forest models to examine potential drivers of hydrologic processes. Random forest models have been  
187 widely used for this task (Eng and Wolock, 2022; Lapidés et al., 2023; Zipper et al., 2021) for their interpretability, relatively  
188 low computational demands, and robustness to multi-collinearity (Addor et al., 2018). For each signature, we constructed a  
189 random forest model to predict its values based on watershed attributes using the caret R package (Kuhn, 2008; R Core Team,  
190 2024). Each model used 500 trees with the optimal number of features randomly resampled at each split, selected by  
191 minimizing root mean squared error (RMSE) through 10-fold cross-validation.

192  
193 Only the signatures calculated from quality-controlled ~~observations streamflow records (as described in Section 3.1)~~ were used  
194 for training. Training on all Caravan watersheds yielded  $R^2 < 0.4$  for many of the signatures, so we limited the training samples  
195 to the 4,748 Caravan watersheds with streamflow gauge IDs overlapping with GAGES-II to attain model performance  
196 comparable to previous studies (see Text S2). ~~Furthermore, we omitted watersheds from our training sample with short or~~  
197 ~~incomplete streamflow records or uncertain watershed boundaries. First, we excluded watersheds with less than 5 years of~~  
198 ~~streamflow observation record, and those with over 30% missing daily data over the period where streamflow was recorded.~~  
199 ~~Second, we removed watersheds from our analysis with uncertain topographic boundaries, showing high discrepancies (>25%)~~  
200 ~~in the estimated drainage area between GAGES-II and Caravan datasets. Third, for overland flow signature analysis, we~~  
201 ~~excluded snow-dominated watersheds (>20% snow fraction of total precipitation); this is because our overland flow signatures~~  
202 ~~can be heavily influenced by periods with no flow response due to snow or frozen conditions.~~ When a gauged watershed was  
203 present in both datasets, we prioritized CAMELS over HYSETS, and Caravan over GAGES-II. This is to ensure the broader  
204 applicability of our method across different countries, as Caravan is available at global scale. This yielded a total 14, ~~146403~~  
205 watersheds for signature analysis (overview in Table S1).

206  
207 We then used the trained model to predict hydrologic signatures for 3,885 watersheds where observations did not meet data  
208 quality standards as described in Section 3.1. Previous study (do Nascimento et al., 2025) and our p Preliminary experiments  
209 (Text S2) showed improved model performance when the watershed attributes were derived from higher-resolution datasets  
210 based on detailed field surveys, such as in GAGES-II and ~~(Holt and McMillan, (2025))~~. Therefore, we used GAGES-II attributes  
211 and when unavailable, used the coarser resolution Caravan attributes (see Table S1).

### 212 3.3 Interpretation of hydrologic signatures as process descriptors

213 We combined signatures calculated from observed streamflow data and predicted with random forest models to develop a  
214 comprehensive map of processes for watersheds across the U.S. (Fig. 1). A bivariate space of hydrologic signatures was used  
215 to infer process dominance. For each selected process, we used the two signatures most strongly related to the process inferred  
216 from previous work (Bolotin and McMillan, 2024; McMillan, 2020; McMillan et al., 2022; Wu et al., 2021). Each signature  
217 was categorized based on the quantiles of signatures, from low (0-25%), mid-low (25-50%), mid-high (50-75%), to high (75-  
218 100%). When both of the two target signatures had mid-high (50-75%) or high (75-100%) values, we interpreted this as  
219 indicative of process dominance. This bivariate matrix can highlight the complexity of hydrologic processes where two  
220 signatures do not necessarily show the same trends.

221  
222 The process hypotheses tested are described in Table 1 and cover six major hydrologic processes: baseflow, watershed storage,  
223 water balance, seasonal variability, overland flow dominance, and its type. Baseflow sustains discharge across seasons and  
224 reflects groundwater connectivity, while overland flow drives stormflow and influences flood peaks. Storage governs buffering

225 and recession dynamics, and water balance losses through evapotranspiration and deep percolation determine how much  
226 precipitation is converted to streamflow. Together, these processes span the continuum from slow to fast hydrologic response  
227 and integrate both vertical and lateral fluxes, making them essential for hydrologic theory and modelling (Bergström, 1992;  
228 Kirchner et al., 2009; Berghuijs et al., 2014).

229  
230 The major process hypotheses are as follows (detailed in Table 1): regions with strong baseflow processes would show high  
231 baseflow magnitude (larger *BFI*) and slow baseflow recession (smaller *recession K*); regions with large storage capacity and  
232 retention would show high storage magnitude (larger *AverageStorage*) and more nonlinear recessions (larger *Recession*  
233 *parameter b*); regions with large water balance losses would show smaller runoff ratios (smaller *TotalRR* and *EventRR*);  
234 regions strongly influenced by seasonality in processes (e.g., evapotranspiration, snow) would show variability in the flow  
235 timeseries and recessions (large *Recession a seasonality* and large *variability index*); regions with strong overland flow or  
236 stormflow processes would exhibit strong threshold responses to precipitation (large *threshold value* and high significance,  
237 small *p*-values); regions dominated by infiltration-excess overland flow would show stronger correlation between flow and  
238 precipitation intensity ( $RC\_Pint > RC\_Pvol$ ) while regions dominated by saturation-excess overland flow would show stronger  
239 correlation between flow and precipitation volume ( $RC\_Pvol > RC\_Pint$ ).

### 240 3.4 Interpretation of process drivers using Shapley values

241 We quantified feature importance using Shapley values (Shapley, 1953), which provide a robust and consistent measure to  
242 interpret random forest models (Lundberg et al., 2018). Shapley values represent the average marginal contribution of a feature  
243 (i.e., a landscape attribute) to a prediction, given the effects from all combinations of the considered features. Shapley values  
244 allow for local and global interpretation of machine learning model predictions, helping to uncover site-specific and  
245 generalizable linkages between hydrology and landscape features (Husic et al., 2025). We used the interpretable machine  
246 learning (iml) R package (Molnar et al., 2018) to calculate Shapley values over the training data.

247  
248 To evaluate the regional effects of watershed attributes, we computed summary statistics on Shapley values. Shapley values  
249 are site-specific:  $\phi_x^{(y,i)}$  is the Shapley value calculated for an attribute  $x$  for a signature  $y$  at location  $i$ . Summing the Shapley  
250 values across watershed attributes  $x$  at a single location gives the deviation of the predicted signature value  $y_i$  at location  $i$  from  
251 the mean signature value across all sites. To compare effects of a landscape attribute  $x$  across sites, we normalize Shapley  
252 values by the total absolute contribution from all attributes at a site  $i$ ; this gives a metric for the relative contribution of an  
253 attribute  $x$  to signature  $y$  at site  $i$  as:

$$R_x^{(y,i)} = |\phi_x^{(y,i)}| / \sum_{x \in A} |\phi_x^{(y,i)}|$$

255 where  $A$  is the set of all watershed attributes, and  $|\cdot|$  denotes the absolute value. To investigate which types of landscape  
256 characteristics are influential, we classified the watershed attributes into five categories (see Table 2), namely, topography,  
257 land-cover, soil & geology, human alteration, and climate.

258

259 Then, the average relative contribution of category  $k$  for signature  $y$  at location  $i$ ,  $\underline{\underline{R}}_k^{(y,i)}$ , is calculated as:

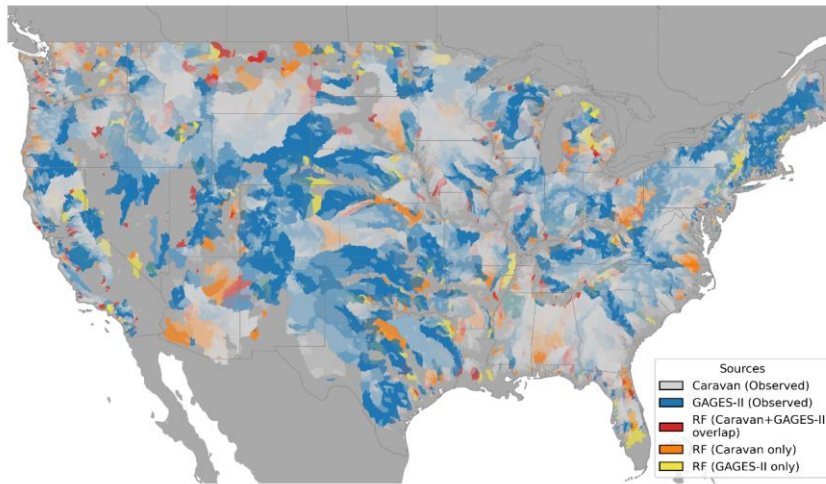
$$\underline{\underline{R}}_k^{(y,i)} = \frac{1}{K} \sum_{x \in C_k} R_x^{(y,i)}$$

261 , where  $C_k$  is the set of watershed attributes belonging to category  $k$ , and  $K$  is the number of categories (in our case, five).

### 262 3.5 Interpretation of process drivers using permutation importance

263 To further evaluate locally important watershed attributes, we computed permutation importance, which measures the change  
264 in model performance when a feature (i.e., a landscape attribute) is removed. Prior work has shown that permutation  
265 importance derived from random forest models trained on regional samples is more effective than a continental approach for  
266 identifying physiographic, landscape controls on hydrologic responses, as it allows assessment under consistent climate  
267 conditions (Almagro et al., 2024; Hammond et al., 2021; Holt and McMillan, 2025). Therefore, we calculated permutation  
268 importance as the average changes in mean squared error (MSE), normalized by its standard deviation using the caret R  
269 package (Kuhn, 2008), from random forest models trained on regional watershed samples. Six climate regions were defined  
270 using a Gaussian mixture model in Scikit-learn (Pedregosa et al., 2011) based on relevant Caravan, GAGES-II, and Hammond  
271 et al. (2023) climate attributes (Table S4), and separate random forest models were trained for each region. Fig. S1 shows the  
272 identified climate regions.

273



274  
275  
276  
277  
278  
279

**Figure 1: Method used to obtain hydrologic signatures.** Signatures are derived either from observed data (“Observed”: Caravan samples, n=7,465; GAGES-II samples, n=2,807; total n=10,261) or predicted using random forest models (“RF”; n=3,885). Predicted samples are categorized as: “Caravan+GAGES-II overlap” (present in both the Caravan and GAGES-II datasets; n=618), “Caravan only” (exclusive to Caravan; n=2,424), and “GAGES-II only” (exclusive to GAGES-II; n=843). State boundaries are indicated by grey lines.

280

## 4 Results

281

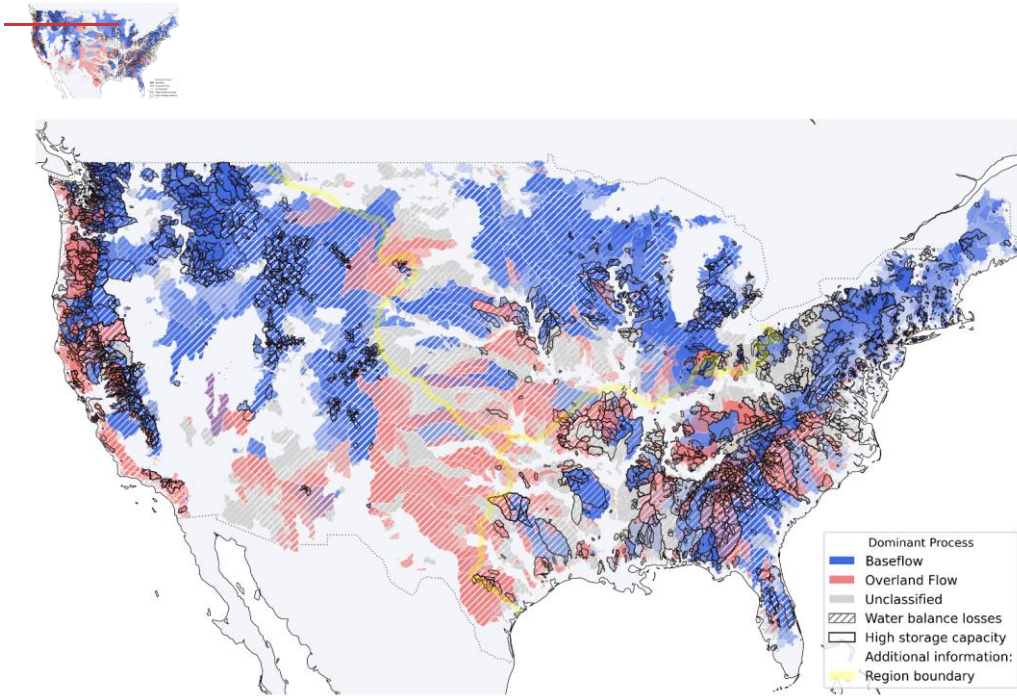
### 4.1 Mapping dominant processes across the contiguous U.S.

282

Figures 2 and 3 show the maps of dominant processes derived from the hypotheses outlined in Table 1. Figure 2 presents the signature of each process hypothesis in a bivariate map. Figure 3 provides a summary, displaying ~~only~~ the four primary hydrologic selected-processes hypothesis when it is deemed dominant (i.e. both signatures are in the mid-high (50-75 %) or high (75-100 %) quantiles). Together, these maps highlight distinct regional patterns in hydrologic processes across the study area. The following sections examine these patterns in greater detail by region: the East and South. (Section 4.2.1.), the Midwest and Central (Section 4.2.2.), and the West and Southwest (Section 4.2.3.).

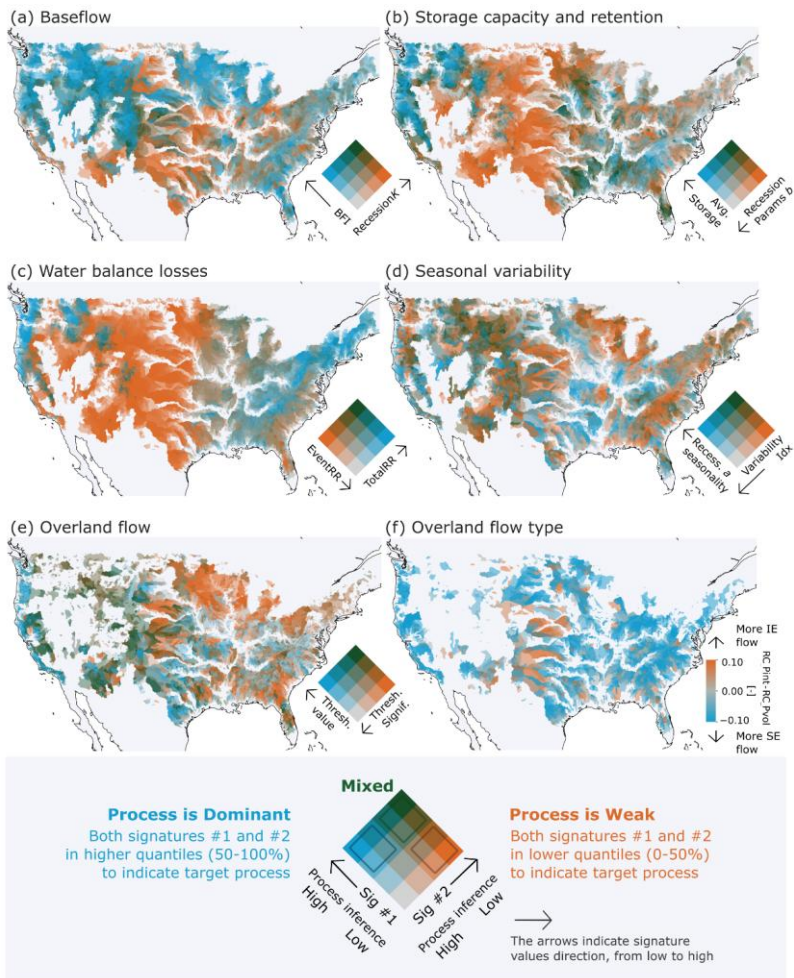
287  
288

289



290

291 **Figure 2: Map of dominant processes estimated based on our hypothesis (defined in Table 1 and Section 3.3). Note that when**  
292 **baseflow and overland flow both occur, their colors are overlaid to give purple hues. “Unclassified” means a watershed is deemed**  
293 **neither baseflow- nor overland-low-dominant. “Region boundary” indicates the areas described in Section 4.2.1-4.2.3 (East and**  
294 **South (bottom right), Midwest and Central, West and Southwest (left in the figure)).**



295

296

297

298

299

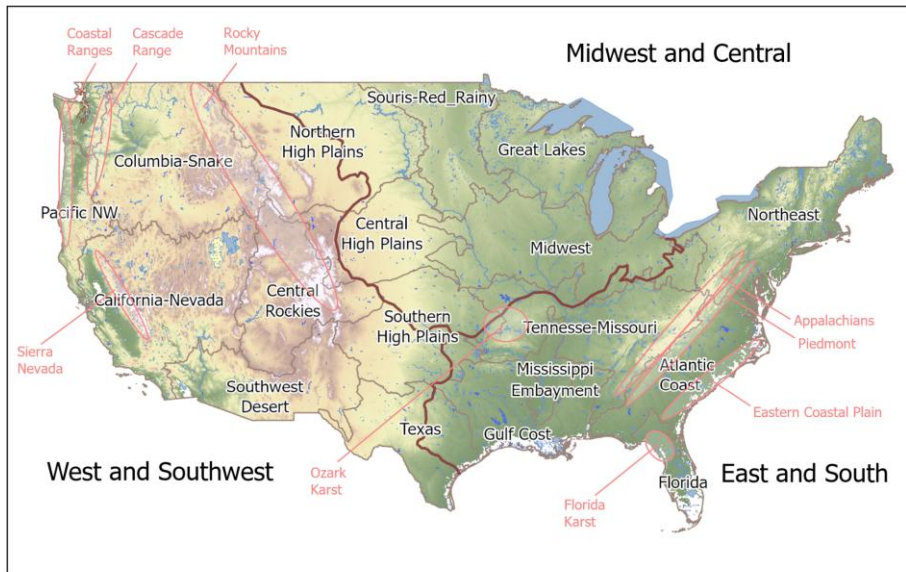
300

301

302

303

**Figure 3: Hydrologic signatures of each process hypothesis, shown in bivariate maps (a-e).** See the legend at the bottom for explanation. The high-process quantile from (a) is used to infer “Baseflow” in Figure 2; from (b) to infer “High storage capacity”; from (c) to infer “Water balance losses”; and from (e) to infer “Overland flow.” Panel (f) shows the differences between the two signatures related to infiltration-excess (IE) flow and saturation-excess (SE) flow (i.e., values of  $RC_{Pint} - PC_{Pvol}$ ). In the overland flow panels (e) and (f), watersheds dominated by snow (i.e., where more than 20% of annual total precipitation falls as snow) are not shown. For the overland flow type pane (f), watersheds are not shown when the correlations between the event runoff coefficient and both rainfall characteristics (i.e., storm rainfall volume and maximum intensity) are negative. For maps of each signature value, see Figures S2 and S3.



304  
 305 **Figure 4: Map of the contiguous United States showing (i) areas described in Section 4.2.1-4.2.3 (East and South, Midwest and**  
 306 **Central, West and Southwest; bolded brown line) (ii) geographical boundaries used for the USGS National Water Availability**  
 307 **Assessment (Qi and Mason, 2023; Stets et al., 2025; Van Metre et al., 2020) (beige line) (iii) topographic and geological features**  
 308 **named in the text (pink annotations).**

309 **4.2 Spatial patterns of hydrologic processes inferred from signatures**

310 **4.2.1 Region 1: East and South**

311 ~~This section describes the East and South of the U.S. (Fig. 4).~~ This humid region has moderate to high precipitation (1,000-  
 312 1,500 mm/yr; calculated based on the 10th and 90th percentiles of sample watershed attributes), with low precipitation  
 313 seasonality except in Florida. Temperatures vary widely from snow-dominated areas in the NorthEast to subtropical areas in  
 314 Florida, with mean annual temperature ranging from 7-19°C (Fig. S4). The landscape is old with deeply weathered soils and  
 315 characterized by predominantly low-lying elevation (mean watershed elevation ranges between 40-600m), though there is a  
 316 primary elevation gradient from the Appalachian Mountains and Piedmont to the Eastern coastal plains, with peaks exceeding  
 317 1,000m (Fig. S8). In Figure 3, signature values show that these climate and landscape conditions produce slowly-varying,  
 318 baseflow-dominated flow regimes and mid-quantile signature values showing a lack of hydrologic extremes. Runoff ratios  
 319 (*TotalRR* and *EventRR*; Fig. 3c) are moderate or high and seasonal variability in flow and recessions is moderate to low.

320 Storage capacity (*Avg. Storage*) is overall moderate, but recession shapes (*Recession Params b*) are variable (Fig. 3b). Evidence  
321 for overland flow is weak with saturation excess prevailing when it occurs (Fig. 3e,f).

322  
323 The gradient along the geographical transect from the Appalachian spine to the Eastern coastal plain is apparent in several  
324 processes. The Appalachians have strong baseflow influence, shown by high baseflow index and slow recessions (Fig. 3a).  
325 Nonlinear recessions (high *Recession Parameter b*; Fig. 3b) indicate multiple groundwater reservoirs supplying baseflow. In  
326 contrast, the Piedmont has lower baseflows and fast recessions, relating to lower storage, ~~a greater fraction of developed land,~~  
327 ~~and wide, wet valley bottoms that generate a fast response (Zimmer and Gannon, 2018).~~ The Eastern coastal plain, especially  
328 towards the South, has high baseflow and moderate to slow recessions (Fig. 3a). Linear recessions suggest a single dominant  
329 groundwater reservoir supplying baseflow ~~in this sandy, coastal plain aquifer (Fig. 3b). These characteristics reflect the sandy~~  
330 ~~soils, seasonal flooding and presence of wetlands atop the coastal plain aquifer (Holt and McMillan, 2025; Hupp, 2000).~~ Lower  
331 runoff ratios in the coastal plains indicate losses to deep groundwater including offshore discharge, especially in Florida's karst  
332 area (Fig. 3c, S6). The karst area stands out for its high dynamic storage and seasonality in recessions. Saturation excess  
333 dominates overland flow in the Coastal plain (Fig. 3f), although evidence for overland flow is weak (Fig. 3e) in contrast to a  
334 previous study (Wieczorek and LaMotte, 2010) that suggests the Florida panhandle has the highest fraction of saturation excess  
335 overland flow in the US.

336  
337 In inland areas such as the valleys of the Tennessee-Missouri region, baseflow is moderate and recessions are relatively fast  
338 (Fig. 3a). The Gulf Coast region has lower baseflow and faster, linear recessions. ~~Although depth to bedrock is high (Fig. S5),~~  
339 ~~and these areas overlie semi-consolidated sand aquifers, soils are clay-rich and capable of generating infiltration excess flow~~  
340 ~~(Miller, 1999; Fig. S6).~~ Infiltration excess flow largely occurs in the narrow ocean margin of the Gulf coast region but does  
341 not extend far inland (Fig. 3f). Exceptions to the area's fast runoff occur in the Ozark Mountains and the west of the Mississippi  
342 embayment where limited areas of high baseflow and slow recessions occur.

#### 343 4.2.2 Region 2: MidWest and Central

344 The landscape of the Midwest and Central region is dominated by the gradient from recently-glaciated, sandy, forested  
345 watersheds of the Great Lakes region, to the poorly-drained, clay-rich but highly developed for agriculture and populated  
346 region of the Souris-Red-Rainy and Midwest regions. Across the Midwest and Central area, mean watershed elevation ranges  
347 from 200 to 700 meters, and mean annual precipitation varies from 500 to 1,000 mm. Moving west into the Central and  
348 Northern High Plain regions, elevation gradually increases, precipitation decreases, and population density decreases (Fig. S8,  
349 S4, S7). The region experiences mean annual temperatures between 6 to 13°C. The absence of major topographic barriers  
350 results in a continental climate characterized by intense thunderstorms in summer and heavy snowfall in winter.

351

Formatted: Not Highlight

352 Signature values show that storage capacity is moderate throughout the Midwest (Fig. 3b). Storage in this region is provided  
353 by a moderate snowpack and high depth to bedrock (Fig. S5). Most of the region was previously glaciated, leaving a thick  
354 layer of glacial drift. The soil texture is graded from coarse and sandy around the Great Lakes to clay-rich further South and  
355 West, forming a distinctive outer ring around the Great Lakes region (Miller and White, 1998; Fig. S6). Following this gradient,  
356 there is ~~very low~~ no significant evidence for overland flow around the Great Lakes, changing to stronger evidence further  
357 South-West (Fig. 3e,f). Some occurrence of infiltration excess is consistent with evidence of this process from Midwest  
358 agricultural watersheds (Abban et al., 2014; Davis et al., 2014; Wilson et al., 2012). Streamflow seasonality follows the same  
359 gradient (Fig. 3d), with low seasonality around the Great Lakes where sandy aquifers sustain discharge year-round, and higher  
360 seasonality further SouthWest (Miller and White, 1998; Fig. 3d). A second gradient occurs in the Midwest from West to East,  
361 following precipitation and aridity gradients (Fig. S4). In the west, high aridity leads to high water balance losses to ET and  
362 low runoff coefficients at the annual and event scale (Fig. 3c).

#### 363 4.2.3 Region 3: West and Southwest

364 The landscape of the West and Southwest region is dominated by the mountain ranges of the Coastal Ranges, Cascades, Sierra  
365 Nevada and Rocky Mountains, with mean watershed elevation ranging from 400 to over 2,700 meters. Dense populations in  
366 the coastal cities give way to sparsely populated inland areas. The climate exhibits strong gradients. The Pacific Northwest  
367 and Sierra Nevada mountain ranges receive substantial amount of precipitation than interior, with mean annual precipitation  
368 ranging from 460 to over 2,100 mm/yr across the region. The region shows a north-south temperature gradient with coastal  
369 moderation. Mean annual temperature ranges from 2°C in northern and high mountain areas to over 20°C in inland southern  
370 desert regions (Fig. S4). Precipitation patterns follow Mediterranean or semi-arid climates characterized by winter precipitation  
371 peaks and dry summers.

372  
373 High baseflows with slow recession are prevalent across most of the Western region, where deep snowpacks drive sustained  
374 baseflow processes (Fig. 3a, S5; Barnhart et al., 2016; Tague and Grant, 2009). Inland areas tend to have faster recessions  
375 while retaining high baseflows, while coastal areas - where snow is rare - have lower baseflow while retaining slow recessions.  
376 The Southwest desert contrasts with the rest of the region, having low baseflows and fast recessions typical of the arid or semi-  
377 arid climate with water tables far below the land surface (Goodrich et al., 1997). Storage capacity and retention follow the  
378 same gradient from high in the Pacific Northwest to low in the South-East, but the high storage region is more constrained to  
379 the Rocky, Cascade and Sierra Nevada mountains (Fig. 3b). Water balance patterns contrast the pattern still further, with only  
380 the high mountains having high runoff ratios in contrast to low ratios throughout the remainder of the Western U.S. (Fig. 3c)  
381 Seasonal variability in processes is higher in the South (primarily California) where the seasonal Mediterranean climate pattern  
382 occurs with hot, dry summers and cool, wet winters (Fig. 3d, S5).

383

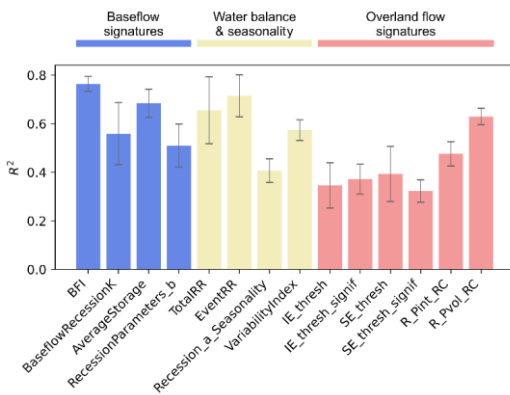
384 Processes in the coastal margin are markedly different from those inland. The moderating influence of the coast is strongly  
 385 apparent in storage capacity (Fig. 3b): the northern Coast Ranges have lower average storage compared to high storage inland  
 386 areas, while the southern coastal band has higher storage compared to low storage inland areas. Overland flows are strongly  
 387 indicated all along the coast, but more weakly inland (Fig. 3c). Most overland flow favors saturation excess, although inland  
 388 watersheds of the Southwest desert show areas of infiltration excess (Fig. 3f).

### 389 4.3 Inferred Climate and landscape drivers of hydrologic processes

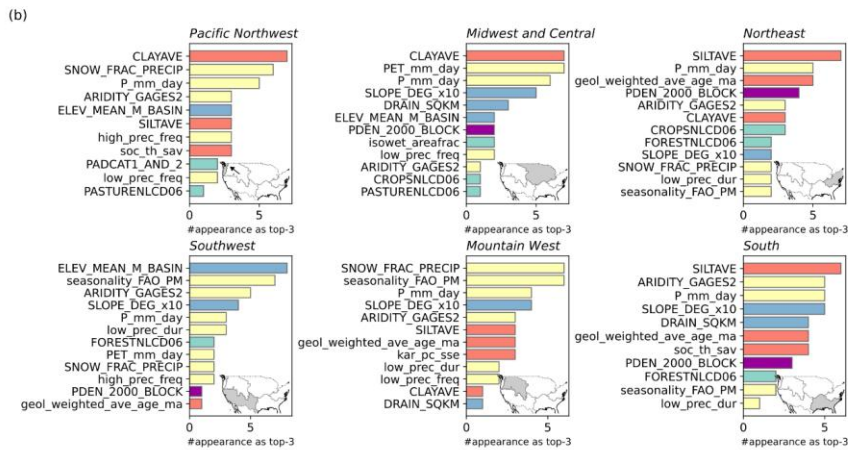
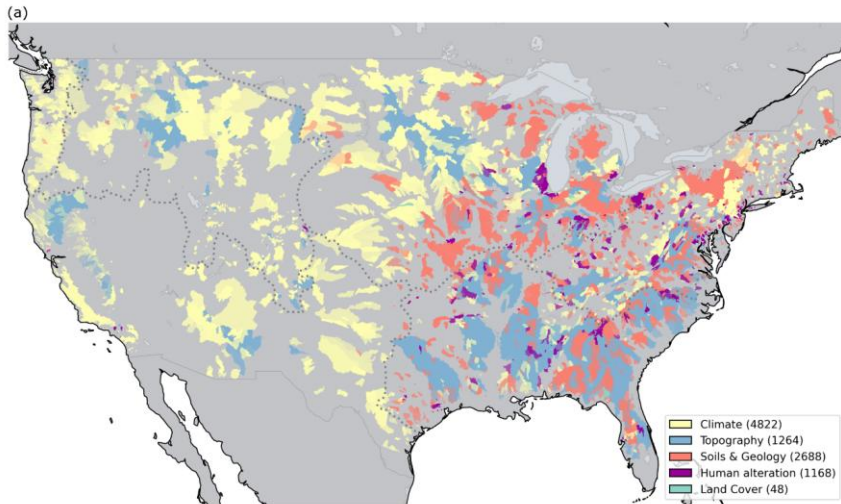
390 In this section, we interpret the random forest models to understand which aspects of climate and landscape are most important  
 391 in controlling hydrologic processes in different regions of the U.S. We hypothesize that variable importance statistics from  
 392 Shapley and permutation analysis reflect the relative importance of hydrologic process drivers. Random forest models  
 393 performed reasonably well ( $R^2 > 0.4$ ) for most signatures (Fig. 5), consistent with previous studies using similar model setups  
 394 (Addor et al., 2018; Beck et al., 2015; Bolotin and McMillan, 2024; Kuentz et al., 2017). Performance was higher for baseflow,  
 395 water balance loss, and seasonality signatures, but lower for overland flow signatures. Figure S9 presents the regional model  
 396 performances for each signature.

Formatted: Font: Not Italic

397  
 398 Figure 6 provides an overview of variable importance results: Figure 6a focuses on spatial patterns, showing the landscape  
 399 attribute category that has the strongest contribution to predictions of signatures and processes for each watershed, calculated  
 400 using aggregated Shapley values; Figures 6b provides deeper insights into the ranking of landscape attributes, ordered by  
 401 permutation importance, for predicting signatures in each region. Figure S10 complements Figure 6a by showing the  
 402 importance of landscape attribute categories in each region, based on permutation importance.



403  
 404 **Figure 5: Ten-fold cross-validation performance of the random forest model trained on 4,748 CONUS-samples, where gauge IDs**  
 405 **overlapped with Caravan and GAGES-II. Bars show the average  $R^2$  between observed and predicted signatures, with error bars**  
 406 **representing the standard deviation. See Table 1 for signature names.**



407  
 408 **Figure 6: (a) The landscape attribute category that contributes most to hydrologic responses was identified based on the average**  
 409 **relative contribution of each category,  $\bar{R}_k^{(y,i)}$  (derived from Shapley values; see Section 3.4). For each watershed, the most important**  
 410 **category  $k$  was determined using the median of  $\bar{R}_k^{(y,i)}$  across all hydrologic signatures. Results are displayed for the watershed**  
 411 **samples included in the random forest training. Numbers in the legend indicate the frequency that each category was identified as**  
 412 **the most important. (b) Frequency of watershed attributes ranked among the top three most important variables in permutation**  
 413 **importance (IncMSE%) across all signatures in six U.S. climate regions. The x-axis indicates how many times each attribute**  
 414 **appeared in the top three. See Section 3.4 and Table 2 for attribute names.**

#### 415 4.3.1 Region 1: East and South

416 In the East and South, a wide variety of landscape attribute categories dominate process predictions, including topography,  
417 soils and geology, climate and human alteration (Fig. 6). Climate attributes dominate in cooler areas in the Northeast and along  
418 the Appalachian spine, while topography attributes dominate on the Eastern coastal plain. Along the Gulf coast, either climate  
419 or soils and geology may dominate. Human alteration attributes dominate clusters of watersheds around cities including New  
420 York, Philadelphia, Washington D.C., Raleigh and Atlanta.

421  
422 Overall, and particularly for signatures relating to storage and water balance in the East and South Region (*TotalRR*, *RR*  
423 *seasonality*, *Event RR*, *AverageStorage*, *RecessionParameters\_b*), the random forest models show that climate drivers are less  
424 important than in the rest of the U.S., and soils and geology, topography, and land cover drivers are more important (Fig. 6,  
425 S10). Human influence (population density) is a more important driver here than in other regions across most signatures,  
426 consistent with large areas of high population (Fig. S7). For example, In addition to the major cities, highly developed areas  
427 of Western Florida have anomalous show anomalous areas of low baseflow, as do developed Piedmont areas (Zimmer and  
428 Gannon, 2018).

429  
430 In the NorthEast, across all signatures, the drivers that most often appeared in the top three controls of random forest  
431 performance were Silt fraction, Precipitation, Geologic Age and Population density — representing the effects of geology,  
432 soils, climate and human development (Fig. 6b). Climate characteristics appear more often for signatures related to water  
433 balance and overland flow. In the South, Silt fraction, Aridity, Precipitation and Slope occur most often, representing gradients  
434 in elevation and soils from the Appalachians to the coastal plain and into Florida (Fig.s S6, S8). These characteristics reflect  
435 the sandy soils, seasonal flooding and presence of wetlands atop the coastal plain aquifer (Holt and McMillan, 2025; Hupp,  
436 2000).

#### 437 4.3.2 Region 2: MidWest and Central

438 In the Midwest and Central area, a wide variety of landscape attribute categories dominate process predictions, including  
439 topography, soils and geology, climate and human alteration, showing strong spatial patterns (Fig. 6). Soils and geology  
440 attributes dominate in the Great Lakes region, and in the arc of clay-rich soils in the High Plains and Midwest regions (Fig.  
441 S6). A mixture of climate and topography attributes dominate in the Souris-Red-Rainy region. Human alteration attributes  
442 dominate in clusters of watersheds around Chicago, Detroit and Cleveland.

443  
444 Overall in the Midwest and Central area, the random forest models show that land cover and topography drivers are more  
445 important than in the rest of the U.S., while climate drivers are less important. Across all signatures, the drivers that most often  
446 appeared in the top three controls of random forest performance were Clay fraction, PET, Precipitation and Slope —

447 representing the effects of soils, climate and topography (Fig. 6); this is consistent with the gradual variation in signatures'  
448 spatial patterns accompanying gradients in glacial drift and climate in this region, as discussed in 4.2.2. Despite the flat  
449 topography of the region, several topographic attributes appear in the top ten, perhaps reflecting the effect of unusual  
450 topographic features such as the driftless area. Land cover metrics (wetland, cropland, pasture) were secondary drivers,  
451 appearing for signatures related to storage and overland flow.

452  
453 The impact of climate is spread between multiple drivers: PET, Precipitation, Low precipitation frequency and Aridity. Climate  
454 drivers in the Midwest and Central area show multiple distinct spatial patterns, with aridity and low precipitation metrics  
455 showing an east-west gradient, temperature and PET having a north-south gradient, and precipitation and seasonality having  
456 a Northwest-Southeast gradient (Fig. S4, S5). Thus, each part of the Midwest and Central area has a unique holistic climate  
457 combination. Climate patterns differ distinctly from the NorthEast-Southwest pattern of the soils and land cover.

#### 458 4.3.3 Region 3: West and Southwest

459 In the West, climate attributes dominate process predictions across most watersheds in the Pacific Northwest and Mountain  
460 West (Fig. 6a, S5). Some mountain areas have dominant topographic attributes, and topography drivers are more important in  
461 the Southwest region compared to the wider U.S.. Climate properties that appear most often include Snow fraction,  
462 Precipitation, Aridity and Seasonality (Fig. 6b: regions Pacific Northwest, Southwest, Mountain West). These attributes  
463 describe the primary climatic features of the West and Southwest U.S., which are governed by precipitation and aridity  
464 gradients from North to South, and from coasts to inland (Fig. S4). Inland mountain chains influence flow regimes by providing  
465 spring snowmelt and mountain block recharge, among the many influences of topography on hydrologic processes (Gnann et  
466 al., 2025). These controls are demonstrated by the importance of snow fraction alongside topographic attributes, elevation and  
467 slope. Soil control on runoff process is seen by the importance of clay fraction in the Pacific Northwest, reflecting Oregon's  
468 common clay soils (Miller and White, 1998).

## 469 5 Discussion

470 This study creates comprehensive maps of hydrologic processes across the contiguous United States by using machine learning  
471 to analyze streamflow signatures ~~from over 10,000 watersheds~~ and connecting these signatures to dominant watershed  
472 processes. The analysis from over 10,000 watersheds shows distinct regional patterns in estimated hydrologic processes and  
473 its potential drivers. The research reveals that climate primarily controls hydrologic processes in the western U.S., while soils  
474 and geology dominate in the Great Lakes region, topography controls processes in the Southeast, and human influences are  
475 most important around large cities across the East. The analysis shows distinct regional patterns in hydrologic processes, with  
476 infiltration excess overland flow dominating the high plains., saturation excess flow prevalent in the valleys of the Tennessee-  
477 Missouri region, and varying baseflow contributions across regions. These process maps provide novel information for

478 selecting appropriate hydrologic models across large domains and help hydrologists anticipate how watersheds will respond  
479 to environmental changes such as altered climate or land use. [In the following sections, we discuss how these maps provide](#)  
480 [new benchmarks \(Section 5.1\), inform hydrologic modelling \(Section 5.2\), and outline directions for future work \(Section 5.3\).](#)

### 481 5.1 New [benchmark maps of process understanding over large domains](#)

482 Our results build on previous work to map hydrologic processes and drivers. Our map of baseflow process importance shows  
483 similar patterns to previous studies into baseflow and groundwater contribution to streamflow (Beck et al., 2013; Santhi et al.,  
484 2008; Xie et al., 2024). As with those studies, our approach of using observations and machine learning methods provides finer  
485 detail than can be estimated using statistical interpolation or by hydrologic or climate models. By combining multiple recent  
486 datasets, we increase the number of observations used in our analysis. In our study, we used >10,000 observed watershed data  
487 within CONUS, representing a substantial advancement compared to the >600 to >3000 observation samples used in previous  
488 studies (Addor et al., 2018; Beck et al., 2013, 2015; Janssen and Ameli, 2021; Wu et al., 2021). Our analysis therefore provides  
489 a new benchmark, offering the most comprehensive coverage and highest spatial characterization of hydrologic processes  
490 across the contiguous United States to date. While larger datasets have been analyzed elsewhere, for example, >8,000  
491 watersheds (Santhi et al., 2008), >23,000 watersheds (Xie et al., 2024), those efforts focused exclusively on baseflow index.  
492 Beck et al. (2013) found sometimes differing drivers of baseflow index and recession slope despite their close connection: by  
493 using bivariate plots, we could more clearly highlight regions where patterns of these two signatures diverge. Those areas  
494 include the Pacific Northwest coast with lower baseflow index but slow recessions, and the central high plains with high  
495 baseflow index but fast recessions.

496  
497 Previous studies investigated patterns of overland flow generation across the U.S. using soil maps and rainfall intensity  
498 (Buchanan et al., 2018) streamflow signatures (Wu et al., 2021) and modeling approaches (Wolock, 2003b). Like us, Buchanan  
499 et al. (2018) and Wu et al., (2021) found infiltration excess runoff important throughout the high plains, and saturation excess  
500 in the valleys of the Tennessee-Missouri region, and a mixture of saturation and infiltration excess in the Southwestern U.S..  
501 Substantial overland flow occurs in Southwest chaparral systems (Valeron and Meixner, 2010), and although deep groundwater  
502 tables suggest infiltration excess, we found a mixture of mechanisms. [This may reflect vegetation shifting the inferred overland](#)  
503 [flow mechanism toward saturation excess. Infiltration excess is inferred when overland flow is related to storm intensity rather](#)  
504 [than storm size. In arid and semi-arid catchments, vegetation can locally increase infiltration capacity and soil water retention,](#)  
505 [reducing the extent of infiltration excess overland flow \(Stein et al., 2021\). Additionally, where smaller storms are intercepted](#)  
506 [by canopies, signatures may incorrectly attribute the runoff to saturation excess rather than infiltration excess. This could be](#)  
507 [due to incorrect inference: where magnitude of overland flow is related to storm size rather than intensity, as smaller storms](#)  
508 [are intercepted by the dense canopy, signatures may incorrectly assign this runoff to saturation excess flow.](#) However, our  
509 results are supported by global studies that show saturation excess is always more common than infiltration excess even in arid

510 regions, as saturation excess is generated in riparian zones and topographic convergence areas where water tables are higher  
511 (McMillan et al., 2025).

512  
513 By mapping and categorizing the primary drivers of runoff processes, we can untangle which physical characteristics drive the  
514 hydrologic response in each region. In the East and South, soil, geology, and topography emerged as primary drivers, which  
515 is consistent with regional hydrologic process knowledge.es: Topography is important in the Appalachian Piedmont, where  
516 wide and wet valley bottoms generate fast responses (Zimmer and Gannon, 2018).; Soils are important clay-rich soils along  
517 the Gulf Coast where clay-rich soils promote infiltration-excess overland flow (Miller, 1999; Fig. S6), producing mixed storage  
518 and water balance signatures despite deep bedrock (Fig. S5) and semi-consolidated sand aquifers; and on the Eastern Coastal  
519 Plain where sandy soils, seasonal flooding, and wetlands likely support a single dominant groundwater reservoir supplying  
520 baseflow (Fig. 3b; Holt and McMillan, 2025; Hupp, 2000). The machine learning approach is especially powerful for this  
521 purpose, as multiple landscape attributes often contribute simultaneously to the hydrologic response. In some areas, there are  
522 multiple landscape attributes that could contribute to the response, for example in the Gulf Coast region the speed of recessions  
523 might be reduced by the high depth to bedrock, but increased by soils with low hydraulic conductivity. We find that silt fraction  
524 (soil texture) drives the response, creating fast recessions, with mapping showing that this is most important along the coastal  
525 margin.

526  
527 Our maps of primary drivers based on Shapley values extend previous work to analyze the drivers of hydrologic signatures.  
528 For example, Addor et al. (2018; their Fig. 3) show that climate (aridity, seasonality, snow fraction) is the primary driver across  
529 most signatures, with topography (elevation, slope) and land cover (forest, leaf area index) being secondary drivers. Figure 6a  
530 similarly shows climate and topography as dominant, but adds spatial information to show that, for example, climate is  
531 dominant in the mountainous western U.S., but soils and geology dominate the Midwest and much of the Northeastern U.S.  
532 Geological age, a recently-proposed attribute to summarize watershed geology, was often in the top random forest attributes  
533 (Holt and McMillan, 2025). This highlights the need and opportunity for development of new landscape attributes that  
534 characterize the subsurface, echoing the call by Tarasova et al. (2023).

535  
536 In four of the six regions, soil texture, particularly silt or clay fraction, was identified as a recurring primary driver (Fig. 6b),  
537 though their roles differ by context. In the Northeast, silt dominates variable importance; silt is found in glacial till layer and  
538 supports high water storage and baseflow (Shanley et al., 2015) while facilitating subsurface stormflow under wet conditions  
539 (Detty and McGuire, 2010). In the South, despite silt being identified as a primary driver, clay is the dominant soil texture in  
540 many areas (Miller and White, 1998); in the Mississippi embayment, extensive confining units of clay and silt separate aquifers  
541 and control the groundwater flow (Renken, 1998; Clark et al., 2011). These two cases suggest that Shapley or permutation-  
542 based methods may not fully separate correlated variables due to their treatment of joint variable distributions, and high clay  
543 content may be implicitly captured through the absence of silt in regional analyses.

## 544 **5.2 Informing model selection and evaluation**

545 Our results support hydrological modeling by enabling hydrologists to check whether key processes in a watershed are well-  
546 represented by a candidate model prior to application. A wide range of hydrologic models with differing process  
547 representations, structures and complexities are available (Knoben et al., 2020). Hydrologists must make choices on whether  
548 to include simulations of additional processes such as snowpack or deep groundwater, and the complexity required such as  
549 including energy balance at the land surface. Our maps of hydrologic processes provide a pre-screening tool to match  
550 hydrological models with appropriate process representations to regions. This approach aims to reduce model structural errors  
551 by discouraging use of models ill-suited to the dominant processes (e.g., using a bucket model in overland flow-dominated  
552 regions).

553

554 Many previous studies have assessed preferred model structure in individual research watersheds, often using in-depth data  
555 analysis to ensure that modeled processes are consistent with observed processes (e.g. Hrachowitz et al., 2014; Kavetski and  
556 Fenicia, 2011). This study provides a method to support transparent model justification in applied studies without the resources  
557 to conduct model structure investigations, and to upscale model structure decisions to large domains. For example, if selecting  
558 models from the MARRMoT toolbox (Knoben et al., 2020), models for regions of dominant overland flow should include  
559 saturation excess and/or infiltration excess pathways, and models for regions of complex storage and retention should include  
560 multiple parallel groundwater reservoirs. The ability to choose appropriate models for thousands of watersheds is needed for  
561 new, flexible model frameworks such as the U.S. Next-Generation National Water Model Framework (Cosgrove et al., 2024;  
562 Johnson et al., 2023; Ogden et al., 2021). Our observation-based method complements previous large-domain model-based  
563 methods that use analysis of model sensitivities (Markstrom et al., 2016) and performance (Prieto et al., 2021; Spieler et al.,  
564 2020) Therefore, where hydrologists seek to evaluate models against process representation, this study offers an opportunity  
565 to enhance model benchmarking frameworks by adding process realism as a metric.

## 566 **5.3 Limitations and future work**

567 The hydrologic process maps produced by this study are limited to the contiguous U.S.. Recent streamflow observation datasets  
568 offer the opportunity to extend this method to other regions or globally. Such datasets include the community Caravan dataset  
569 (Kratzert et al., 2023), and the international dataset of watersheds with limited human influences, Reference Observatory of  
570 Basins for International hydrological climate change detection (ROBIN; Turner et al., 2025). If extending the method globally,  
571 caution is advised with scaling, in order to represent different ranges of signature values in different regions. In this study, we  
572 plotted signature values as quantiles based on the U.S. distribution, but other countries may have very different signature  
573 distributions (McMillan et al., 2022). Therefore, watershed processes that are considered important in a U.S. context, may be  
574 considered less important in a global context. Further, some regions of the U.S. are excluded or poorly represented in the  
575 dominant process maps presented in this paper, due to a low spatial coverage of USGS stream gages. For example, there are

576 significant gaps in the arid southwest where perennial streamflow is rare (Kiang et al., 2013; Krabbenhoft et al., 2022). In such  
577 regions there is a need for alternative process-mapping methods that do not rely on streamflow records.

578  
579 Hydrological signatures in this study are long-term averages of the multi-year streamflow dynamics, which may not fully  
580 capture temporal variability in watershed processes. Future studies should account for long-term hydroclimatic changes  
581 (Hobeichi et al., 2022; Gudmundsson et al., 2025), as well as inter-annual variability (Vogel et al., 1994) and seasonal  
582 variations in watershed function (Payn et al., 2012; Gomi et al., 2008). Another complication is that hydrologic signatures are  
583 often confounded by multiple processes (McMillan et al., 2020, 2023), whether weather driven by natural flow dynamics or  
584 impaired by human activities. For example, water abstraction by reservoirs reduces downstream flow variability and increases  
585 water balance deficits (Salwey et al., 2022; Veldkamp et al., 2016), but changes in vegetation or climate could induce similar  
586 effects. Disentangling these impacts remains challenging without testing narrower hypotheses about watershed function,  
587 incorporating expert knowledge, or having detailed information about human interventions. In this study, we partially mitigated  
588 this issue by using multiple signatures to characterize processes, and by representing human alteration through population  
589 density, which showed strong explanatory power for the signatures. Nevertheless, considerable effort is still needed to isolate  
590 the combined impacts of multiple processes, as well as the effects of urban development and agricultural practices on flow  
591 dynamics (Grantham et al., 2022) for improving the large-scale application of signatures.

592  
593 A limitation of this study that would become more apparent at a global scale is the quality of precipitation, streamflow, and  
594 attribute data. A previous study noted issues with limited quality and consistency of the global attribute data for soils and  
595 geology that reduced their predictive power (Beck et al., 2015). Continental scales necessitate the use of gridded precipitation  
596 products, but in areas with low density of observations these products may be insufficient to analyze localized, flashy processes  
597 such as infiltration excess flow (McMillan et al., 2023). In small, headwater watersheds, precipitation grid size may be large  
598 compared to watershed area, and headwaters are also underrepresented in streamflow observations (Golden et al., 2025).  
599 Additionally, errors in watershed boundary delineation would affect signatures that use drainage area to normalize flow, such  
600 as runoff ratio (*TotalRR*, *EventRR*) and water balance (*AverageStorage*). In snowy areas, signature values can be compromised  
601 because liquid water inputs to the watershed come from snowmelt rather than directly from precipitation. In our study, we  
602 excluded snow-dominated watersheds for signatures related to overland flow, as these require event-scale surface water input  
603 that are particularly affected by frozen or snowmelt conditions. Products such as NLDAS3 (Case et al., 2025) or surface water  
604 inputs considering rain-on-snow and snowmelt (Hammond, 2024; Hammond and Kampf, 2020) may provide future abilities  
605 to estimate overland flow processes in snow areas using estimates of hourly snow accumulation and melt. While our study  
606 used potential evapotranspiration (PET) information in only one signature (*AverageStorage*), uncertainty in PET is a major  
607 issue of global datasets and needs to be addressed (Clerc-Schwarzenbach et al., 2024; Destouni and Zarei, 2024) before this  
608 approach can be expanded to a variety of (eco)hydrologic processes.

Formatted: Font: Italic

Formatted: Font: Italic

Formatted: Font: Italic

610 A further limitation is the extent to which continental scale maps of dominant processes can be validated. Large-domain  
611 signature datasets can be evaluated for data quality, for interpolation quality using cross-validation, and compared with  
612 previous datasets. However, it is more difficult to determine how accurately signatures relate to processes over large domains.  
613 Research watersheds offer “ground truth” points at which processes are already well understood (Penna, 2024). Previous  
614 studies used a handful of U.S. critical zone observatory watersheds for evaluation (McMillan et al., 2022). However, the large  
615 number of past and present research watersheds across the globe offer an interesting future opportunity for wider-scale  
616 validation of process mapping techniques (McMillan et al., 2025; Sebestyen et al., 2025). Similarly, validation of process  
617 drivers remains challenging. While Shapley values and permutation importance provide explanatory power for random forest  
618 models, they have some limitations. Both metrics characterize model interactions within a given dataset; therefore, the variety  
619 of processes covered in the dataset matters, and data or model uncertainties may propagate into the interpretations (Husic,  
620 2025). Shapley values do not capture joint distributional effects among multiple interacting variables (Lundberg and Lee,  
621 2017). Developing an explanatory framework that maximizes both model performance and interpretability remains an ongoing  
622 research area in hydrology (Robert Maier et al., 2024; Willard et al., 2024).

## 623 **6.5 Conclusion**

624 A fundamental question in hydrology is how hydrologic processes are organized over large scales, and how they are controlled  
625 by climate and landscape (Blöschl et al., 2019). In this study, we contribute towards answering this question by mapping  
626 hydrologic processes and their drivers across the contiguous U.S.. Our approach used hydrologic signatures to describe  
627 streamflow dynamics, and connected these dynamics to dominant processes in the associated watersheds using established  
628 relationships between signatures and watershed processes. We analyzed 14,146 gauged U.S. watersheds; our map of processes  
629 was based on observational data from 10,261 gauged sites and extended using random forest predictions to an additional 3,885  
630 watersheds with insufficient record length or completeness. Our method enables knowledge transfer from gauged basins with  
631 well-established conceptual models to ungauged or poorly instrumented watersheds.

632  
633 Our results comprise maps of hydrologic process importance across the contiguous U.S., including baseflow, overland flow,  
634 water storage, seasonal variation and water balance processes. Using interpretable machine learning methods, we create maps  
635 of process drivers that explain which climate and landscape attributes are dominant in controlling hydrologic processes in each  
636 watershed and each region. ~~We find clear patterns at the continental scale –analysis shows distinct regional patterns in~~  
637 ~~hydrologic processes, with infiltration excess overland flow dominating the high plains., saturation excess flow prevalent in~~  
638 ~~the valleys of the Tennessee-Missouri region, and varying baseflow contributions across regions. The research further reveals~~  
639 ~~that climate primarily controls hydrologic processes in the western U.S., while soils and geology dominate in the Great Lakes~~  
640 ~~region, topography controls processes in the Southeast, and human influences are most important around large cities across~~  
641 ~~the East. We find clear patterns at the continental scale, such that processes most strongly relate to climate in the western U.S.,~~

642 ~~to soils and geology in the Great Lakes region, to topography in the Southeast, and to human influences around large cities,~~  
643 ~~especially in the Northeast.~~

644  
645 Our findings extend and generalize process understanding from research watersheds to large domains, revealing regional  
646 heterogeneity within broader physiographic provinces that are often treated as hydrologically uniform. Hydrologic process  
647 maps provide essential support for new, large-domain model frameworks that must select model structure across thousands of  
648 watersheds. These maps enable hydrologists to select models that adequately represent the dominant processes of a watershed.  
649 Identification of dominant processes in each region further enables hydrologists to anticipate streamflow response to  
650 environmental change, by identifying which processes are most sensitive to shifts in driving variables. Such analysis has the  
651 potential to support scenario testing for future land use or climate, to guide selection of green and grey infrastructure compatible  
652 with dominant processes, and to inform risk assessments for regions prone to flash flooding, streamflow depletion, or altered  
653 seasonal flow regimes.

#### 654 **Code availability**

655 Code used for analysis is available via Zenodo at (*The Zenodo link will be made available following the revision and upon*  
656 *completion of the publication-ready version*) and as a continuously updated version via GitHub at  
657 <https://github.com/RY4GIT/signature-prediction>. Code used to calculate geologic and wetland attributes (Holt and McMillan,  
658 2025) is deposited in Zenodo at (*The Zenodo link will be made available following the revision and upon completion of the*  
659 *publication-ready version*) and as a continuously updated version via GitHub  
660 at [https://github.com/RY4GIT/Wetland\\_GeologicAge\\_Attributes](https://github.com/RY4GIT/Wetland_GeologicAge_Attributes). Caravan attributes for GAGES-II only watersheds were  
661 calculated using <https://github.com/kratzert/Caravan> (Kratzert et al., 2023). Hydrologic signatures are calculated using  
662 <https://github.com/RY4GIT/TOSSH>, which modified the original TOSSH toolbox <https://github.com/TOSSHtoolbox/TOSSH>  
663 (Gnann et al., 2021b).

#### 664 **Data availability**

665 The hydrologic signature datasets, derived from observed data and predicted using random forest models, are deposited at (*The*  
666 *Hydroshare link will be made available following the revision and upon completion of the publication-ready version*). The  
667 Caravan Version 1.5 dataset is available at <https://doi.org/10.5281/zenodo.10968468> (Kratzert et al., 2024), which contains  
668 streamflow, meteorological data, watershed boundaries and attributes. GAGES-II attributes are available at  
669 <https://www.sciencebase.gov/catalog/item/631405bbd34e36012efa304a> (Falcone, 2011), and time series of meteorological  
670 data for GAGES-II locations are available from <https://www.sciencebase.gov/catalog/item/64134069d34eb496d1cc3c6f>  
671 (Wieczorek et al., 2023) and <https://www.sciencebase.gov/catalog/item/6494515fd34cf77fcb014eb0> (Hammond, 2024).

672 CAMELSH hourly NLDAS forcings are available at <https://doi.org/10.5281/zenodo.15066778> and  
673 <https://doi.org/10.5281/zenodo.15070091> (Tran et al., 2025).

#### 674 **Author contribution**

675 **Araki:** conceptualization, data curation, formal analysis, investigation, methodology, software, visualization, writing —  
676 original draft preparation, writing — review and editing. **Holt:** conceptualization, data curation, methodology, software, writing  
677 — review and editing. **Hammond:** data curation, formal analysis, methodology, writing — original draft preparation, writing  
678 — review and editing. **Husic:** formal analysis, investigation, methodology, writing — original draft preparation, writing —  
679 review and editing. **Coxon:** investigation, writing — review and editing. **McMillan:** funding acquisition, project administration,  
680 conceptualization, formal analysis, investigation, methodology, writing — original draft preparation, writing — review and  
681 editing, supervision.

#### 682 **Competing interests**

683 At least one of the (co-)authors is a member of the editorial board of Hydrology and Earth System Sciences. The peer-review  
684 process was guided by an independent editor, and the authors also have no other competing interests to declare.

#### 685 **Acknowledgement**

686 We thank Sebastian Gnann for the development of the TOSSH toolbox and for the collaborative discussions around my pull  
687 requests, ~~and~~ Yueling Ma for helpful input on interpretable Machine Learning methods during a conference, ~~and~~ [Andy Wood](#)  
688 [for valuable feedback about anthropogenic impacts on streamflow patterns and signatures](#). The bivariate map was inspired by  
689 a blogpost written by Muhammad Mohsin Raza on their website DataWim. We thank Roy Sando and Scott Hamshaw for  
690 helpful feedback on the earlier version of the manuscript. We appreciate the computing support provided by the IT team at the  
691 Department of Geography, San Diego State University, and the General Research IT (GRIT) team at the University of  
692 California, Santa Barbara. Any use of trade, firm, or product names is for descriptive purposes only and does not imply  
693 endorsement by the U.S. government.

#### 694 **Financial Support**

695 Araki, Holt, McMillan were supported by the NSF Hydrologic Sciences Program, Division of Earth Sciences, Award Number  
696 2124923. Araki acknowledges support from the Shida Scholarship Program. Coxon was supported by a UKRI Future Leaders  
697 Fellowship [MR/V022857/1].  
698

700 **Table 1:** Hydrologic signatures used for building process hypotheses. The signature descriptions are adapted from  
 701 (McMillan et al., 2022).

Hydrologic processes and signature hypothesis	Relationship between the signature values and process strength	Signature	Unit	Description
<b>Baseflow</b>  We hypothesize that a larger baseflow magnitude (i.e., higher <i>BFI</i> ) and a slower recession rate (i.e., lower <i>BaseflowRecessionK</i> ) indicate a stronger baseflow process.	Positive	<i>BFI</i>	-	Baseflow index (BFI) represents baseflow proportion and residence time (Bulygina et al., 2009; Yilmaz et al., 2008). Calculated as mean baseflow divided by mean streamflow. Hydrograph separation is implemented to obtain baseflow fraction using the UKIH smoothed minima method (UKIH, 1980).
	Negative	<i>BaseflowRecessionK</i>	1/d	Represents groundwater influence and longer subsurface flow paths (Safeeq et al., 2013). Calculated as an exponential recession constant K fitted to the master recession curve derived from adaptive matching strip method.
<b>High storage capacity</b>  We hypothesize that larger storage (i.e., higher <i>AverageStorage</i> ) and more nonlinear recession behavior patterns (i.e., higher <i>RecessionParameters_b</i> ) indicate a greater storage capacity and the involvement of multiple storages.	Positive	<i>AverageStorage</i>	mm	Represents average magnitude of watershed storage (Peters and Aulenbach, 2011). Derived from average baseflow and storage-discharge relationship. Uses a simple water balance model to calculate changes in storage, then finds the relationship between storage and discharge, and then estimates average storage from average baseflow.
	Positive	<i>RecessionParameters_b</i>	-	The nonlinearity indicates the contributions of multiple storages (Clark et al., 2009; Tallaksen, 1995). Recession analysis parameters approximate storage-discharge relationship. Fits a line to the $dQ/dt$ -Q relationship in log-log space for each individual recession and returns the median slope. <i>b</i> is a shape parameter representing the degree of nonlinearity.
<b>Water balance losses</b>  We hypothesize that a smaller runoff ratio (Q:P ratio) at both interannual and event scales (i.e., lower <i>TotalRR</i> and <i>EventRR</i> ) indicates greater water balance losses due to evapotranspiration, deep drainage to groundwater, or some other processes.	Negative	<i>TotalRR</i>	-	Total runoff ratio (RR) infer evapotranspiration or other flow bypassing gauge (Safeeq and Hunsaker, 2016). Calculated as mean streamflow divided by mean precipitation.
	Negative	<i>EventRR</i>	-	Event runoff ratio (RR) infer rapid vertical drainage of water to groundwater (Noguchi et al., 1997). Calculated as an average of runoff ratios (streamflow divided by precipitation) from all identified storm events.

<b>Seasonal variability</b>  We hypothesize that greater flow variability, both in general patterns (i.e., higher <i>Variability Index</i> ) and in seasonal patterns (i.e., higher <i>Recession_a_Seasonality</i> ), indicates a stronger influence of seasonal evapotranspiration patterns on water storage.	Positive	<i>Recession_a_Seasonality</i>	-	Seasonal variation in the recession “a” parameter reflects the impact of evapotranspiration on water storage (Shaw and Riha, 2012). Calculated as the difference between the maximum and minimum monthly median values of the y-intercept (“a” parameter) in the $dQ/dt-Q$ relationship in log-log space, assuming a slope of 2.
	Positive	<i>VariabilityIndex</i>	-	High variability index shows lower water storage (Estrany et al., 2010). Calculated as the standard deviation of log-transformed discharge values determined at 10% intervals from 10% to 90% of the cumulative frequency distribution (flow duration curve).
<b>Overland flow</b>  We hypothesized that a strong threshold relationship between quickflow and precipitation characteristics (i.e., high significance and higher threshold values) suggests a more dominant overland flow process.	<p>Negative (Values outside the range <math>0 \leq p\text{-value} \leq 0.05</math> are deemed insignificant and clipped out. Within the range, the smaller P-value is, the more significant the threshold is)</p> <p>Negative (Values outside the range <math>0 \leq P\text{-value} \leq 0.05</math> are deemed insignificant and clipped out. Within the range, the smaller P-value is, the more significant the threshold is)</p>	<i>Average of IE_thresh_signif and SE_thresh_signif</i>	-	Significant values ( $<0.05$ ) imply infiltration excess (IE) or saturation excess (SE) occurs (Ali et al., 2013; McGrath et al., 2007). <i>p</i> -value was calculated for the significance of a non-zero change in slope above and below a threshold in a relationship of event quickflow volume versus event maximum precipitation intensity (for IE) or event total precipitation volume (for SE).
	Positive	<i>Average of IE_thresh and SE_thresh</i>	mm	Indicates rainfall intensity or event precipitation depth required to generate infiltration excess or saturation excess, respectively (Ali et al., 2013; McGrath et al., 2007). Value of the threshold identified in the IE/SE_thresh_signif signature. The “broken-stick” model was fit to the relationship between quickflow vs. precipitation characteristics.
<b>Overland flow type</b>  We hypothesized that the relative strength in infiltration vs. saturation of excess overland flow (i.e., differences	Positive relationship with infiltration excess overland flow	<i>RC_Pvol</i>	-	Indicates stormflow processes sensitive to rainfall intensity, for example, infiltration excess (Hortonian) overland flow (Wu et al., 2021). Calculated as the Spearman correlation coefficients between event runoff coefficient and event maximum rainfall intensity. As <i>pe</i> (Wu et al.,

<p>in <math>RC_{Pvol}</math> and <math>RC_{Pint}</math> indicate the prevalence of either overland flow mechanisms.</p> <p>Exclude watersheds where event runoff coefficient has negative relationships with storm characteristics (i.e., <math>RC_{Pvol} &lt; 0</math> and <math>RC_{Pint} &lt; 0</math>).</p>				<p>2021), event maximum rainfall intensity is calculated as the multiplication of daily rainfall (mm/day) from original climate forcings (i.e., ERA5 for Caravan, gridMET for GAGES-II) multiplied by the fraction of maximum rainfall intensity from CAMELSH hourly NLDAS forcings.</p>
	<p>Positive relationship with saturation excess overland flow</p>	<p><math>RC_{Pint}</math></p>	<p>-</p>	<p>Indicates stormflow processes sensitive to rainfall volume, for example, saturation excess overland flow, subsurface stormflow, and groundwater flow (Wu et al., 2021). Calculated as the Spearman correlation coefficients between event runoff coefficient and rainfall volume.</p>

702

703

704 **Table 2:** Landscape attributes used in training the random forest model. Descriptions are adapted from (Falcone, 2011;  
705 Falcone et al., 2010; Holt and McMillan, 2025; Kratzert et al., 2023; Linke et al., 2019). For predictions, when certain  
706 attributes are unavailable, equivalent attributes are substituted (e.g., Caravan equivalents are used when predicting signatures  
707 for watershed samples available only in Caravan). The combinations are detailed in Table S1. An asterisk (\*) in the unit  
708 column indicates that the landscape attribute unit from GAGES-II was converted to the Caravan equivalent (Fig. S11 shows  
709 the comparison).  
710

Category	Attribute Name	Description	Unit	Original Source	Dataset Source	Caravan Equivalent
Physiography	ELEV_MEAN_M_BASIN	Mean watershed elevation	meters	USGS 100m National Elevation Dataset (Gesch et al., 2018)	GAGES-II	ele_mt_sav
Physiography	DRAIN_SQ KM	Watershed drainage area	km <sup>2</sup>	Multiple sources, while the majority derived from NHDPlus (U.S. Environmental Protection Agency, 2008) (see original USGS, 2011 report on GAGES-II)	GAGES-II	area
Physiography	SLOPE_PCT	Mean watershed slope, percent	%	USGS 100m resolution National Elevation Dataset (Gesch et al., 2018)	GAGES-II	slp_dg_sav
Land Cover	FORESTNL CD06	Forest extent	% area	NLCD06 for most regions; NLCD01 for Alaska, Hawaii, and Puerto Rico (Yang et al., 2018)	GAGES-II	for_pc_sse
Land Cover	CROPSNLC D06	Cultivated Crops extent	% area		GAGES-II	crp_pc_sse
Land Cover	PASTUREN LCD06	Pasture/Hay extent	% area		GAGES-II	pst_pc_sse
Land Cover	PCT_IRRIG_AG	Irrigated agriculture extent	% area	Based on 250m MODIS datasets, USGS M1rAD-US (Shrestha et al., 2019)	GAGES-II	ire_pc_sse
Land Cover	PADCAT1_AND_2	Percent of watershed designated as Protected Area Category 1 and 2	% area *	Protected Areas Database (United States Geological Survey, 2024)	GAGES-II	pac_pc_sse

Land Cover	isowet_areafraction	Isolated wetland area fraction (Holt, 2024)	-	National Wetlands Inventory (Lane and D'Amico, 2016)	Holt and McMillan, 2025	N/A
Soils & Geology	CLAYAVE	Average clay content	%	STATSGO (United States Department of Agriculture et al., 2008)	GAGES-II	cly_pc_sav
Soils & Geology	SILTAVE	Average silt content	%		GAGES-II	slt_pc_sav
Soils & Geology	soc_th_sav	Organic carbon content in soil	tonnes/hectare		Caravan/HydroAtlas	N/A
Soils & Geology	kar_pc_sse	Karst area extent	% area	Rock Outcrops v3.0 (Williams and Ford, 2006)	Caravan/HydroAtlas	N/A
Soils & Geology	geol_weighted_average_age_ma	Area-weighted average of geologic age	ma	The USGS State Geologic Map Compilation (Horton et al., 2017)	Holt and McMillan, 2025	N/A
Anthropogenic	PDEN_2000_BLOCK	Population density in the watershed	persons/km <sup>2</sup>	2000 Census block data regridded to 100m	GAGES-II	ppd_pk_sav
Climate	P_mm_day	Mean annual precipitation (1971-2000). The unit was converted from the original variable "PPTAVG_BASIN" in cm/year to mm/day.	mm/day *	800m PRISM data	GAGES-II	p_mean
Climate	PET_mm_day	Mean annual potential evapotranspiration rate estimated from mean monthly air temperature and latitude using Hamon (1961) equation. The unit was converted from the original variable "PET" in mm/year to mm/day.	mm/day *	Monthly air temperature from 30-year (1961-1990) PRISM	GAGES-II	pet_mean_FAO_PM
Climate	ARIDITY_GAGES2	Aridity index, ratio of mean PET and mean precipitation	-	Calculated from PPTAVG_BASIN and PET in GAGES-II attributes	GAGES-II	aridity_FAO_PM
Climate	SNOW_PCT_PRECIP	Mean snow percent of total precipitation estimate (1901-2000)	- *	McCabe and Wolock (submitted, 2008), 1km grid	GAGES-II	frac_snow

Climate	seasonality_FAO_PM	Moisture index seasonality in range [0, 2] (Knoben et al., 2018), where 0 indicates no change in the water or energy budget throughout the year, and 2 indicates a transition from fully arid to fully humid conditions. The moisture index is calculated as the normalized aridity index at the monthly scale.	-	ERA-5 (Muñoz Sabater, 2019); The FAO Penman–Monteith equation (Allen et al., 1998; Shalev and Kratzert, 2024) is used to calculate Potential Evapotranspiration (PET)	Caravan/ERA-5	N/A
Climate	high_prec_freq	<b>Frequency of high precipitation days, where precipitation <math>\geq 5</math> times mean daily precipitation</b>  <u>Frequency of high precipitation days, where precipitation <math>&gt; 5</math> times mean daily precipitation</u>	-	ERA-5 (Muñoz Sabater, 2019)	Caravan/ERA-5	N/A
Climate	low_prec_freq	Frequency of low precipitation days, where precipitation $< 1$ mm/day	-	ERA-5 (Muñoz Sabater, 2019)	Caravan/ERA-5	N/A
Climate	low_prec_dur	Average duration of low precipitation events (number of consecutive days where precipitation $< 1$ mm/day)	day	ERA-5 (Muñoz Sabater, 2019)	Caravan/ERA-5	N/A

## 711 References

- 712 Abban, B., Papanicolaou, A. N. (thanos), Cowles, M. K., and Wilson, C. G.: Examining Seasonal Trends in Sediment Source  
713 Contributions in an Intensely Cultivated Midwestern Sub-Watershed Using Bayesian Unmixing, in: World Environmental and  
714 Water Resources Congress 2014, World Environmental and Water Resources Congress 2014, Portland, Oregon, 1453–1463,  
715 <https://doi.org/10.1061/9780784413548.146>, 2014.
- 716 Addor, N., Newman, A. J., Mizukami, N., and Clark, M. P.: The CAMELS data set: catchment attributes and meteorology for  
717 large-sample studies, *Hydrol. Earth Syst. Sci.*, 21, 5293–5313, <https://doi.org/10.5194/hess-21-5293-2017>, 2017.
- 718 Addor, N., Nearing, G., Prieto, C., Newman, A. J., Le Vine, N., and Clark, M. P.: A ranking of hydrological signatures based  
719 on their predictability in space, *Water Resour. Res.*, 54, 8792–8812, <https://doi.org/10.1029/2018WR022606>, 2018.
- 720 Ali, G., Tetzlaff, D., Soulsby, C., McDonnell, J. J., and Capell, R.: A comparison of similarity indices for catchment  
721 classification using a cross-regional dataset, *Adv. Water Resour.*, 40, 11–22, <https://doi.org/10.1016/j.advwatres.2012.01.008>,  
722 2012.

723 Ali, G., Oswald, C. J., Spence, C., Cammeraat, E. L. H., McGuire, K. J., Meixner, T., and Reaney, S. M.: Towards a unified  
724 threshold-based hydrological theory: necessary components and recurring challenges: INVITED COMMENTARY, *Hydrol.*  
725 *Process.*, 27, 313–318, <https://doi.org/10.1002/hyp.9560>, 2013.

726 Allen, R. G., Pereira, L. S., Raes, D., and Smith, M.: Crop Evapotranspiration – Guidelines for Computing Crop Water  
727 Requirements, in: *FAO Irrigation and drainage paper 56*, Food and Agriculture Organization of the United Nations, Rome,  
728 Italy, 1998.

729 Almagro, A., Meira Neto, A. A., Vergopolan, N., Roy, T., Troch, P. A., and Oliveira, P. T. S.: The Drivers of Hydrologic  
730 Behavior in Brazil: Insights From a Catchment Classification, *Water Resources Research*, 60,  
731 <https://doi.org/10.1029/2024WR037212>, 2024.

732 Angermann, L., Jackisch, C., Allroggen, N., Sprenger, M., Zehe, E., Tronicke, J., Weiler, M., and Blume, T.: Form and function  
733 in hillslope hydrology: characterization of subsurface flow based on response observations, *Hydrol. Earth Syst. Sci.*, 21, 3727–  
734 3748, <https://doi.org/10.5194/hess-21-3727-2017>, 2017.

735 Araki, R., Branger, F., Wickenkamp, I., and McMillan, H. K.: A signature-based approach to quantify soil moisture dynamics  
736 under contrasting land-uses, *Hydrol. Process.*, 36, e14553, <https://doi.org/10.1002/hyp.14553>, 2022.

737 Ariano, S. and Ali, G.: From river flow regime diversity to proxies for hydrologic homogeneity a Canada-wide case study, *Sci.*  
738 *Rep.*, 15, 16743, <https://doi.org/10.1038/s41598-025-00244-7>, 2025.

739 Arsenault, R., Brissette, F., Martel, J.-L., Troin, M., Lévesque, G., Davidson-Chaput, J., Gonzalez, M. C., Ameli, A., and  
740 Poulin, A.: A comprehensive, multisource database for hydrometeorological modeling of 14,425 North American watersheds,  
741 *Sci Data*, 7, 243, <https://doi.org/10.1038/s41597-020-00583-2>, 2020.

742 Barnhart, T. B., Molotch, N. P., Livneh, B., Harpold, A. A., Knowles, J. F., and Schneider, D.: Snowmelt baseflow  
743 contributions: A comparison of methods using nested catchments in the Colorado River basin, *Water Resources Research*, 52,  
744 4524–4548, 2016.

745 Barnhart, T. B., Farmer, W. H., Hammond, J. C., Sextstone, G. A., Curran, J. H., Koch, J. C., and Driscoll, J. M.: Evaluating  
746 hydrologic region assignment techniques for unaged basins in Alaska, USA, *River Res. Appl.*, 38, 1569–1584,  
747 <https://doi.org/10.1002/rra.4028>, 2022.

748 Beck, H., Dijk, A., Miralles, D., Jeu, R. A. M., (Sampurno) Bruijnzeel, L., McVicar, T., and Schellekens, J.: Global patterns  
749 in base flow index and recession based on streamflow observations from 3394 catchments, *Water Resources Research*, 49,  
750 7843–7863, <https://doi.org/10.1002/2013WR013918>, 2013.

751 Beck, H. E., De Roo, A., and van Dijk, A. I.: Global maps of streamflow characteristics based on observations from several  
752 thousand catchments, *J. Hydrometeorol.*, 16, 1478–1501, 2015.

753 [Bergström, S.: The HBV Model: Its Structure and Applications, Swedish Meteorological and Hydrological Institute \(SMHI\),](#)  
754 [Hydrology, Norrköping, 35 pp., 1992.](#)

755 Berghuijs, W. R., Sivapalan, M., Woods, R. A., and Savenije, H. H. G.: Patterns of similarity of seasonal water balances: A  
756 window into streamflow variability over a range of time scales, *Water Resour. Res.*, 50, 5638–5661,  
757 <https://doi.org/10.1002/2014WR015692>, 2014.

758 Blöschl, G.: Hydrologic synthesis: Across processes, places, and scales, *Water Resour. Res.*, 42,  
759 <https://doi.org/10.1029/2005wr004319>, 2006.

760 Blöschl, G., Bierkens, M. F. P., Chambel, A., Cudennec, C., Destouni, G., Fiori, A., Kirchner, J. W., McDonnell, J. J., Savenije,  
761 H. H. G., Sivapalan, M., Stumpp, C., Toth, E., Volpi, E., Carr, G., Lupton, C., Salinas, J., Széles, B., Viglione, A., Aksoy, H.,  
762 Allen, S. T., Amin, A., Andréassian, V., Arheimer, B., Aryal, S. K., Baker, V., Bardsley, E., Barendrecht, M. H., Bartosova,  
763 A., Batelaan, O., Berghuijs, W. R., Beven, K., Blume, T., Bogaard, T., Borges de Amorim, P., Böttcher, M. E., Boulet, G.,  
764 Breinl, K., Brilly, M., Brocca, L., Buytaert, W., Castellarin, A., Castelletti, A., Chen, X., Chen, Y., Chen, Y., Chiffard, P.,  
765 Claps, P., Clark, M. P., Collins, A. L., Croke, B., Dathe, A., David, P. C., de Barros, F. P. J., de Rooij, G., Di Baldassarre, G.,  
766 Driscoll, J. M., Duethmann, D., Dwivedi, R., Eris, E., Farmer, W. H., Feiccabrino, J., Ferguson, G., Ferrari, E., Ferraris, S.,  
767 Fersch, B., Finger, D., Foglia, L., Fowler, K., Gartsman, B., Gascoïn, S., Gaume, E., Gelfan, A., Geris, J., Gharari, S., Gleeson,  
768 T., Glendell, M., Gonzalez Bevacqua, A., González-Dugo, M. P., Grimaldi, S., Gupta, A. B., Guse, B., Han, D., Hannah, D.,  
769 Harpold, A., Haun, S., Heal, K., Helfricht, K., Herrnegger, M., Hipsey, M., Hlaváčiková, H., Hohmann, C., Holko, L.,  
770 Hopkinson, C., Hrachowitz, M., Illangasekare, T. H., Inam, A., Innocente, C., Istanbuluoglu, E., Jarhani, B., et al.: Twenty-  
771 three unsolved problems in hydrology (UPH) – a community perspective, *Hydrol. Sci. J.*, 64, 1141–1158,  
772 <https://doi.org/10.1080/02626667.2019.1620507>, 2019.

773 Bolotin, L. A. and McMillan, H.: A hydrologic signature approach to analysing wildfire impacts on overland flow, *Hydrol.*  
774 *Process.*, 38, <https://doi.org/10.1002/hyp.15215>, 2024.

775 Bracken, L. J., Wainwright, J., Ali, G. A., Tetzlaff, D., Smith, M. W., Reaney, S. M., and Roy, A. G.: Concepts of hydrological  
776 connectivity: Research approaches, pathways and future agendas, *Earth-Sci. Rev.*, 119, 17–34,  
777 <https://doi.org/10.1016/j.earscirev.2013.02.001>, 2013.

778 Brooks, P. D., Chorover, J., Fan, Y., Godsey, S. E., Maxwell, R. M., McNamara, J. P., and Tague, C.: Hydrological partitioning  
779 in the critical zone: Recent advances and opportunities for developing transferable understanding of water cycle dynamics:  
780 CRITICAL ZONE HYDROLOGY, *Water Resour. Res.*, 51, 6973–6987, <https://doi.org/10.1002/2015wr017039>, 2015.

781 Brunner, M. I., Melsen, L. A., Newman, A. J., Wood, A. W., and Clark, M. P.: Future streamflow regime changes in the United  
782 States: assessment using functional classification, *Hydrol. Earth Syst. Sci.*, 24, 3951–3966, [https://doi.org/10.5194/hess-24-](https://doi.org/10.5194/hess-24-3951-2020)  
783 [3951-2020](https://doi.org/10.5194/hess-24-3951-2020), 2020.

784 Buchanan, B., Auerbach, D. A., Knighton, J., Evensen, D., Fuka, D. R., Easton, Z., Wiczorek, M., Archibald, J. A.,  
785 McWilliams, B., and Walter, T.: Estimating dominant runoff modes across the conterminous United States, *Hydrol. Process.*,  
786 32, 3881–3890, <https://doi.org/10.1002/hyp.13296>, 2018.

787 Bulygina, N., McIntyre, N., and Wheatler, H.: Conditioning rainfall-runoff model parameters for ungauged catchments and  
788 land management impacts analysis, *Hydrol. Earth Syst. Sci.*, 13, 893–904, <https://doi.org/10.5194/hess-13-893-2009>, 2009.

789 Case, J. L., Mocko, D. M., Hain, C. R., Maina, F. Z., Whitney, K. M., Kumar, S. V., Wade, R. A., Locke, K. A., and White,  
790 K. D.: NLDAS-3: Next-Generation Land Data Assimilation System to Support North American Water-Informed Decisions,  
791 in: 2025 National Soil Moisture Workshop, 2025.

792 Clark, M., Rupp, D., Woods, R., Meerveld, H., Peters, N., and Freer, J.: Consistency between hydrological models and field  
793 observations: linking processes at the hillslope scale to hydrological responses at the watershed scale, *Hydrological Processes*,  
794 23, 311–319, <https://doi.org/10.1002/HYP.7154>, 2009.

795 Clark, M., Nijssen, B., Lundquist, J., Kavetski, D., Rupp, D., Woods, R., Freer, J., Gutmann, E., Wood, A., Brekke, L., Arnold,  
796 J., Gochis, D., and Rasmussen, R.: A unified approach for process-based hydrologic modeling: 1. Modeling concept, *Water  
797 Resources Research*, 51, 2498–2514, <https://doi.org/10.1002/2015WR017198>, 2015.

798 Clerc-Schwarzenbach, F., Selleri, G., Neri, M., Toth, E., van Meerveld, I., and Seibert, J.: Large-sample hydrology – a few  
799 camels or a whole caravan?, *Hydrol. Earth Syst. Sci.*, 28, 4219–4237, <https://doi.org/10.5194/hess-28-4219-2024>, 2024.

800 [Clark, B. R., Hart, R. M., and Gurdak, J.J.: Groundwater Availability of the Mississippi Embayment, U.S. Geological Survey,  
801 Reston, Professional Paper 1785, 62p.](#)

802 Cosgrove, B., Gochis, D., Flowers, T., Dugger, A., Ogden, F., Graziano, T., Clark, E., Cabell, R., Casiday, N., Cui, Z., Eicher,  
803 K., Fall, G., Feng, X., Fitzgerald, K., Frazier, N., George, C., Gibbs, R., Hernandez, L., Johnson, D., Jones, R., Karsten, L.,  
804 Kefelegn, H., Kitzmiller, D., Lee, H., Liu, Y., Mashriqui, H., Mattern, D., McCluskey, A., McCreight, J. L., McDaniel, R.,  
805 Midekisa, A., Newman, A., Pan, L., Pham, C., RafieeiNasab, A., Rasmussen, R., Read, L., Rezaeianzadeh, M., Salas, F., Sang,  
806 D., Sampson, K., Schneider, T., Shi, Q., Sood, G., Wood, A., Wu, W., Yates, D., Yu, W., and Zhang, Y.: NOAA's National  
807 Water Model: Advancing operational hydrology through continental-scale modeling, *J. Am. Water Resour. Assoc.*, 60, 247–  
808 272, <https://doi.org/10.1111/1752-1688.13184>, 2024.

809 Davis, C. A., Ward, A. S., Burgin, A. J., Loecke, T. D., Riveros-Iregui, D. A., Schnoebelen, D. J., Just, C. L., Thomas, S. A.,  
810 Weber, L. J., and St. Clair, M. A.: Antecedent Moisture Controls on Stream Nitrate Flux in an Agricultural Watershed, *Journal  
811 of Environmental Quality*, 43, 1494–1503, <https://doi.org/10.2134/jeq2013.11.0438>, 2014.

812 DeCicco, L. A., Hirsch, R. M., Lorenz, D., Watkins, D., and Michael Johnson, J.: dataRetrieval, U.S. Geological Survey,  
813 <https://doi.org/10.5066/P9X4L3GE>, 2018.

814 Destouni, G. and Zarei, M.: Water and climate interplay on land in comparative datasets: Revealing unrealistic major drying  
815 bias of climate reanalysis over Africa and the world, *AGUFM*, 2024, H54B–05, 2024.

816 Dettinger, M. D. and Diaz, H. F.: Global characteristics of stream flow seasonality and variability, *J. Hydrometeorol.*, 1, 289–  
817 310, [https://doi.org/10.1175/1525-7541\(2000\)001<0289:gcofs>2.0.co;2](https://doi.org/10.1175/1525-7541(2000)001<0289:gcofs>2.0.co;2), 2000.

818 [Detty, J. M. and McGuire, K. J.: Threshold changes in storm runoff generation at a till-mantled headwater catchment, \*Water  
819 Resour. Res.\*, 46, <https://doi.org/10.1029/2009wr008102>, 2010.](#)

820 Dhungel, S., Tarboton, D. G., Jin, J., and Hawkins, C. P.: Potential effects of climate change on ecologically relevant  
821 streamflow regimes: Climate change and streamflow regimes, *River Res. Appl.*, 32, 1827–1840,  
822 <https://doi.org/10.1002/rra.3029>, 2016.

823 [do Nascimento, T. V., Rudlang, J., Gnann, S., Seibert, J., Hrachowitz, M., & Fenicia, F.: How do geological map details](#)  
824 [influence the identification of geology-streamflow relationships in large-sample hydrology studies? \*Hydrol. Earth Syst. Sci.\*](#)  
825 [29\(24\), 7173-7200. <https://doi.org/10.5194/hess-29-7173-2025>, 2025.](#)

826 Eng, K. and Wolock, D. M.: Evaluation of machine learning approaches for predicting streamflow metrics across the  
827 conterminous United States, 2022–5058, 2022.

828 Estrany, J., Garcia, C., and Batalla, R. J.: Hydrological response of a small mediterranean agricultural catchment, *J. Hydrol.*  
829 (Amst.), 380, 180–190, <https://doi.org/10.1016/j.jhydrol.2009.10.035>, 2010.

830 Falcone, J.: GAGES-II: Geospatial Attributes of Gages for Evaluating Streamflow, <https://doi.org/10.5066/P96CPHOT>, 2011.

831 Falcone, J. A., Carlisle, D. M., Wolock, D. M., and Meador, M. R.: GAGES: A stream gage database for evaluating natural  
832 and altered flow conditions in the conterminous United States, *Ecology*, 91, 621–621, <https://doi.org/10.1890/09-0889.1>, 2010.

833 Fang, K. and Shen, C.: Full-flow-regime storage-streamflow correlation patterns provide insights into hydrologic functioning  
834 over the continental US, *Water Resour. Res.*, 53, 8064–8083, <https://doi.org/10.1002/2016wr020283>, 2017.

835 Fan, Y., Clark, M., Lawrence, D. M., Swenson, S., Band, L. E., Brantley, S. L., Brooks, P. D., Dietrich, W. E., Flores, A.,  
836 Grant, G., Kirchner, J. W., Mackay, D. S., McDonnell, J. J., Milly, P. C. D., Sullivan, P. L., Tague, C., Ajami, H., Chaney, N.,  
837 Hartmann, A., Hazenberg, P., McNamara, J., Pelletier, J., Perket, J., Rouholahnejad-Freund, E., Wagener, T., Zeng, X.,  
838 Beighley, E., Buzan, J., Huang, M., Livneh, B., Mohanty, B. P., Nijssen, B., Safeeq, M., Shen, C., Verseveld, W., Volk, J.,  
839 and Yamazaki, D.: Hillslope hydrology in global change research and Earth system modeling, *Water Resour. Res.*, 55, 1737–  
840 1772, <https://doi.org/10.1029/2018wr023903>, 2019.

841 Fenicia, F. and McDonnell, J. J.: Modeling streamflow variability regional scale:(1) perceptual model development through  
842 signature analysis, *Journal Hydrology*, 2022.

843 Frame, J. M., Araki, R., Bhuiyan, S. A., Bindas, T., Rapp, J., Bolotin, L., Deardorff, E., Liu, Q., Haces-Garcia, F., Liao, M.,  
844 Frazier, N., and Ogden, F. L.: Machine learning for a heterogeneous water modeling framework, *J. Am. Water Resour. Assoc.*,  
845 61, <https://doi.org/10.1111/1752-1688.70000>, 2025.

846 Gesch, D. B., Evans, G. A., Oimoen, M. J., and Arundel, S.: The National Elevation Dataset: USGS Earth Resources  
847 Observation and Science Center, 2018.

848 Gnann, S., Baldwin, J. W., Cuthbert, M. O., Gleeson, T., Schwanghart, W., and Wagener, T.: The influence of topography on  
849 the global terrestrial water cycle, *Rev. Geophys.*, 63, e2023RG000810, <https://doi.org/10.1029/2023rg000810>, 2025.

850 Gnann, S. J., Howden, N. J. K., and Woods, R. A.: Hydrological signatures describing the translation of climate seasonality  
851 into streamflow seasonality, *Hydrol. Earth Syst. Sci. Discuss.*, 24, 561–580, <https://doi.org/10.5194/hess-24-561-2020>, 2020.

852 Gnann, S. J., McMillan, H. K., Woods, R. A., and Howden, N. J. K.: Including Regional Knowledge Improves Baseflow  
853 Signature Predictions in Large Sample Hydrology, *Water Resour. Res.*, 57, e2020WR028354,  
854 <https://doi.org/10.1029/2020WR028354>, 2021a.

855 Gnann, S. J., Coxon, G., Woods, R. A., Howden, N. J. K., and McMillan, H. K.: TOSSH: A Toolbox for Streamflow Signatures  
856 in Hydrology, *Environmental Modelling & Software*, 138, 104983, <https://doi.org/10.1016/j.envsoft.2021.104983>, 2021b.

857 Golden, H. E., Christensen, J. R., McMillan, H. K., Kelleher, C. A., Lane, C. R., Husic, A., Li, L., Ward, A. S., Hammond, J.,  
858 Seybold, E. C., Jaeger, K. L., Zimmer, M., Sando, R., Jones, C. N., Segura, C., Mahoney, D. T., Price, A. N., and Cheng, F.:  
859 Advancing the science of headwater streamflow for global water protection, *Nat Water*, 1–11, [https://doi.org/10.1038/s44221-](https://doi.org/10.1038/s44221-024-00351-1)  
860 [024-00351-1](https://doi.org/10.1038/s44221-024-00351-1), 2025.

861 [Gomi, T., Sidle, R. C., Ueno, M., Miyata, S., & Kosugi, K. \(2008\). Characteristics of overland flow generation on steep](#)  
862 [forested hillslopes of central Japan. \*Journal of Hydrology\*, 361\(3-4\), 275-290. <https://doi.org/10.1016/j.jhydrol.2008.07.045>](#)

863 Goodrich, D. C., Lane, L. J., Shillito, R. M., Miller, S. N., Syed, K. H., and Woolhiser, D. A.: Linearity of basin response as a  
864 function of scale in a semiarid watershed, *Water Resour. Res.*, 33, 2951–2965, <https://doi.org/10.1029/97wr01422>, 1997.

865 [Grantham, T. E., Carlisle, D. M., Howard, J., Lane, B., Lusardi, R., Obester, A., Sandoval-Solis, S., Stanford, B., Stein, E. D.,](#)  
866 [Taniguchi-Quan, K. T., Yarnell, S. M., and Zimmerman, J. K. H.: Modeling functional flows in California’s rivers, \*Front.\*](#)  
867 [\*Environ. Sci.\*, 10, <https://doi.org/10.3389/fenvs.2022.787473>, 2022.](#)

868 [Gudmundsson, L., Brunner, M. I., Döll, P., Fluet-Chouinard, E., Frolova, N., Gosling, S. N., Hirabayashi, Y., Kireeva, M. B.,](#)  
869 [Liu, X., Müller Schmied, H., Magritskiy, D., Slater, L. J., Stein, L., Trambly, Y., Wang, K., Wasko, C., Yamazaki, D., and](#)  
870 [Zhou, X.: Past and future change in global river flows, \*Nat. Rev. Earth Environ.\*, \[https://doi.org/10.1038/s43017-025-00745-\]\(https://doi.org/10.1038/s43017-025-00745-z\)](#)  
871 [z](https://doi.org/10.1038/s43017-025-00745-z), 2025.

872 Haines, A., Finlayson, B., and McMahon, T.: A global classification of river regimes, *Applied Geography*, 8, 255–272,  
873 [https://doi.org/10.1016/0143-6228\(88\)90035-5](https://doi.org/10.1016/0143-6228(88)90035-5), 1988.

874 Hammond, J. C.: Daily time series of surface water input from rainfall, rain on snow, and snowmelt for the Conterminous  
875 United States from 1990 to 2023, as well as annual series of input seasonality, precipitation seasonality, and average rainfall,  
876 rain on snow, and snowmelt rates, <https://doi.org/10.5066/P9JWJPNC>, 2024.

877 Hammond, J. C. and Kampf, S. K.: Subannual streamflow responses to rainfall and snowmelt inputs in snow-dominated  
878 watersheds of the western United States, *Water Resour. Res.*, 56, <https://doi.org/10.1029/2019wr026132>, 2020.

879 Hammond, J. C., Zimmer, M., Shanfield, M., Kaiser, K., Godsey, S. E., Mims, M. C., Zipper, S. C., Burrows, R. M., Kampf,  
880 S. K., Dodds, W., Jones, C. N., Krabbenhoft, C. A., Boersma, K. S., Datry, T., Olden, J. D., Allen, G. H., Price, A. N., Costigan,  
881 K., Hale, R., Ward, A. S., and Allen, D. C.: Spatial patterns and drivers of nonperennial flow regimes in the contiguous United  
882 States, *Geophys. Res. Lett.*, 48, <https://doi.org/10.1029/2020gl090794>, 2021.

883 Hammond, J. C., Sexstone, G. A., Putman, A. L., Barnhart, T. B., Rey, D. M., Driscoll, J. M., Liston, G. E., Rasmussen, K. L.,  
884 McGrath, D., Fassnacht, S. R., and Kampf, S. K.: High resolution SnowModel simulations reveal future elevation-dependent  
885 snow loss and earlier, flashier surface water input for the upper Colorado river basin, *Earths Future*, 11,  
886 <https://doi.org/10.1029/2022ef003092>, 2023.

887 Hay, L. E., LaFontaine, J. H., Van Beusekom, A. E., Norton, P. A., Farmer, W. H., Regan, R. S., Markstrom, S. L., and  
888 Dickinson, J. E.: Parameter estimation at the conterminous United States scale and streamflow routing enhancements for the  
889 National Hydrologic Model infrastructure application of the Precipitation-Runoff Modeling System (NHM-PRMS),  
890 <https://doi.org/10.3133/tm6b10>, 2023.

891 [Hobeichi, S., Abramowitz, G., Ukkola, A. M., De Kauwe, M., Pitman, A., Evans, J. P., and Beck, H.: Reconciling historical](#)  
892 [changes in the hydrological cycle over land, \*Npj Clim. Atmos. Sci.\*, 5, 17, <https://doi.org/10.1038/s41612-022-00240-y>, 2022.](#)  
893 Hodgkins, G. A., Renard, B., Whitfield, P. H., Laaha, G., Stahl, K., Hannaford, J., Burn, D. H., Westra, S., Fleig, A. K., Araújo  
894 Lopes, W. T., Murphy, C., Mediero, L., and Hanel, M.: Climate driven trends in historical extreme low streamflows on four  
895 continents, *Water Resour. Res.*, 60, <https://doi.org/10.1029/2022wr034326>, 2024.  
896 Holt, A.: New Predictors for Hydrologic Signatures: Wetlands and Geologic Age Across Continental Scales, San Diego State  
897 University, United States -- California, 2024.  
898 Holt, A. and McMillan, H.: New predictors for hydrologic signatures: Wetlands and geologic age across continental scales,  
899 *Hydrol. Process.*, 39, <https://doi.org/10.1002/hyp.70080>, 2025.  
900 Horton, J. D., San Juan, C. A., and Stoesser, D. B.: The State Geologic Map Compilation (SGMC) geodatabase of the  
901 conterminous United States, <https://doi.org/10.3133/ds1052>, 2017.  
902 Hrachowitz, M., Fovet, O., Ruiz, L., Euser, T., Gharari, S., Nijzink, R., Freer, J., Savenije, H. H. G., and Gascuel-Odoux, C.:  
903 Process consistency in models: The importance of system signatures, expert knowledge, and process complexity, *Water Resour.*  
904 *Res.*, 50, 7445–7469, <https://doi.org/10.1002/2014wr015484>, 2014.  
905 Hupp, C. R.: Hydrology, geomorphology and vegetation of Coastal Plain rivers in the south-eastern USA. *Hydrological*  
906 *processes*, 14, 2991–3010, 2000.  
907 Husic, A.: Game theory for catchment science, ESS Open Archive, <https://doi.org/10.22541/essoar.173924202.27840286/v1>,  
908 2025.  
909 Husic, A., Hammond, J., Price, A. N., and Roundy, J. K.: Interrogating process deficiencies in large-scale hydrologic models  
910 with interpretable machine learning, *Hydrol. Earth Syst. Sci.*, 29, 4457–4472, <https://doi.org/10.5194/hess-29-4457-2025>,  
911 2025.  
912 Jackisch, C., Angermann, L., Allroggen, N., Sprenger, M., Blume, T., Tronicke, J., and Zehe, E.: Form and function in hillslope  
913 hydrology: in situ imaging and characterization of flow-relevant structures, *Hydrol. Earth Syst. Sci.*, 21, 3749–3775, 2017.  
914 Janssen, J. and Ameli, A. A.: A hydrologic functional approach for improving large-sample hydrology performance in poorly  
915 gauged regions, *Water Resour. Res.*, 57, <https://doi.org/10.1029/2021wr030263>, 2021.  
916 Jefferson, A., Grant, G. E., Lewis, S. L., and Lancaster, S. T.: Coevolution of hydrology and topography on a basalt landscape  
917 in the Oregon Cascade Range, USA, *Earth Surf. Process.*, <https://doi.org/10.1002/esp.1976>, 2010.  
918 Ji, H., Song, Y., Bindas, T., Shen, C., Yang, Y., Pan, M., Liu, J., Rahmani, F., Abbas, A., Beck, H., Lawson, K., and Wada,  
919 Y.: Distinct hydrologic response patterns and trends worldwide revealed by physics-embedded learning, *arXiv [physics.geo-*  
920 *ph]*, arXiv, 2025.  
921 Johnson, J. M., Fang, S., Sankarasubramanian, A., Rad, A. M., Kindl da Cunha, L., Jennings, K. S., Clarke, K. C., Mazrooei,  
922 A., and Yeghiazarian, L.: Comprehensive analysis of the NOAA National Water Model: A call for heterogeneous formulations  
923 and diagnostic model selection, *J. Geophys. Res.*, 128, <https://doi.org/10.1029/2023jd038534>, 2023.

924 Kavetski, D. and Fenicia, F.: Elements of a flexible approach for conceptual hydrological modeling: 2. Application and  
925 experimental insights, *Water Resour. Res.*, 47, <https://doi.org/10.1029/2011wr010748>, 2011.

926 Kennard, M. J., Pusey, B. J., Olden, J. D., Mackay, S. J., Stein, J. L., and Marsh, N.: Classification of natural flow regimes in  
927 Australia to support environmental flow management: Classification of natural flow regimes in Australia, *Freshw. Biol.*, 55,  
928 171–193, <https://doi.org/10.1111/j.1365-2427.2009.02307.x>, 2010.

929 Kiang, J. E., Stewart, D. W., Archfield, S. A., Osborne, E. B., and Eng, K.: A national streamflow network gap analysis (No.  
930 2013-5013), US Geological Survey, 2013.

931 [Kirchner, J. W.: Catchments as simple dynamical systems: Catchment characterization, rainfall-runoff modeling, and doing](https://doi.org/10.1029/2008WR006912)  
932 [hydrology backward. \*Water Resources Research\*, 45\(2\). <https://doi.org/10.1029/2008WR006912>. 2009.](https://doi.org/10.1029/2008WR006912)

933 Knoben, W. J. M., Woods, R. A., and Freer, J. E.: A quantitative hydrological climate classification evaluated with independent  
934 streamflow data, *Water Resour. Res.*, 54, 5088–5109, <https://doi.org/10.1029/2018wr022913>, 2018.

935 Knoben, W. J. M., Freer, J. E., Peel, M. C., Fowler, K. J. A., and Woods, R. A.: A brief analysis of conceptual model structure  
936 uncertainty using 36 models and 559 catchments, *Water Resour. Res.*, 56, e2019WR025975,  
937 <https://doi.org/10.1029/2019wr025975>, 2020.

938 Krabbenhoft, C. A., Allen, G. H., Lin, P., Godsey, S. E., Allen, D. C., Burrows, R. M., DelVecchia, A. G., Fritz, K. M.,  
939 Shanafield, M., Burgin, A. J., Zimmer, M. A., Detry, T., Dodds, W. K., Jones, C. N., Mims, M. C., Franklin, C., Hammond, J.  
940 C., Zipper, S., Ward, A. S., Costigan, K. H., Beck, H. E., and Olden, J. D.: Assessing placement bias of the global river gauge  
941 network, *Nat. Sustain.*, 5, 586–592, <https://doi.org/10.1038/s41893-022-00873-0>, 2022.

942 Kratzert, F., Nearing, G., Addor, N., Erickson, T., Gauch, M., Gilon, O., Gudmundsson, L., Hassidim, A., Klotz, D., Nevo, S.,  
943 Shalev, G., and Matias, Y.: Caravan - A global community dataset for large-sample hydrology, *Sci Data*, 10, 61,  
944 <https://doi.org/10.1038/s41597-023-01975-w>, 2023.

945 Kratzert, F., Nearing, G., Addor, N., Erickson, T., Gauch, M., Gilon, O., Gudmundsson, L., Hassidim, A., Klotz, D., Nevo, S.,  
946 Shalev, G., and Matias, Y.: Caravan - A global community dataset for large-sample hydrology Version 1.4,  
947 <https://doi.org/10.5281/ZENODO.10968468>, 2024.

948 Kuentz, A., Arheimer, B., Hundecha, Y., and Wagener, T.: Understanding hydrologic variability across Europe through  
949 catchment classification, *Hydrol. Earth Syst. Sci.*, 21, 2863–2879, 2017.

950 Kuhn, M.: Building predictive models in R using the caret package, *Journal of Statistical Software*, 28, 1–26,  
951 <https://doi.org/10.18637/JSS.V028.I05>, 2008.

952 Lane, B. A., Dahlke, H. E., Pasternack, G. B., and Sandoval-Solis, S.: Revealing the Diversity of Natural Hydrologic Regimes  
953 in California with Relevance for Environmental Flows Applications, *J. Am. Water Resour. Assoc.*, 53, 411–430,  
954 <https://doi.org/10.1111/1752-1688.12504>, 2017.

955 Lane, C. R. and D'Amico, E.: Identification of putative geographically isolated wetlands of the conterminous United States, *J.*  
956 *Am. Water Resour. Assoc.*, 52, 705–722, <https://doi.org/10.1111/1752-1688.12421>, 2016.

957 Lapides, D. A., Zipper, S., and Hammond, J. C.: Identifying hydrologic signatures associated with streamflow depletion caused  
958 by groundwater pumping, *Hydrol. Process.*, 37, <https://doi.org/10.1002/hyp.14877>, 2023.

959 Lee, D., Ward, P., and Block, P.: Defining high-flow seasons using temporal streamflow patterns from a global model, *Hydrol.*  
960 *Earth Syst. Sci.*, 19, 4689–4705, <https://doi.org/10.5194/hess-19-4689-2015>, 2015.

961 Linke, S., Lehner, B., Ouellet Dallaire, C., Ariwi, J., Grill, G., Anand, M., Beames, P., Burchard-Levine, V., Maxwell, S.,  
962 Moidu, H., Tan, F., and Thieme, M.: Global hydro-environmental sub-basin and river reach characteristics at high spatial  
963 resolution, *Sci Data*, 6, 283, <https://doi.org/10.1038/s41597-019-0300-6>, 2019.

964 Lins, H. F.: Regional streamflow regimes and hydroclimatology of the United States, *Water Resour. Res.*, 33, 1655–1667,  
965 <https://doi.org/10.1029/97WR00615>, 1997.

966 Lohse, K. A. and Dietrich, W. E.: Contrasting effects of soil development on hydrological properties and flow paths, *Water*  
967 *Resour. Res.*, 41, <https://doi.org/10.1029/2004wr003403>, 2005.

968 Lundberg, S. and Lee, S.-I.: A unified approach to interpreting model predictions, *arXiv [cs.AI]*, arXiv, 2017.

969 Lundberg, S. M., Erion, G. G., and Lee, S.-I.: Consistent individualized feature attribution for tree ensembles, *arXiv [cs.LG]*,  
970 arXiv, 2018.

971 Markstrom, S. L., Hay, L. E., and Clark, M. P.: Towards simplification of hydrologic modeling: identification of dominant  
972 processes, *Hydrol. Earth Syst. Sci.*, 20, 4655–4671, <https://doi.org/10.5194/hess-20-4655-2016>, 2016.

973 Mazvimavi, D., Meijerink, A. M. J., Savenije, H. H. G., and Stein, A.: Prediction of flow characteristics using multiple  
974 regression and neural networks: A case study in Zimbabwe, *Phys. Chem. Earth (2002)*, 30, 639–647,  
975 <https://doi.org/10.1016/j.pce.2005.08.003>, 2005.

976 McGrath, G. S., Hinz, C., and Sivapalan, M.: Temporal dynamics of hydrological threshold events, *Hydrol. Earth Syst. Sci.*,  
977 11, 923–938, <https://doi.org/10.5194/hess-11-923-2007>, 2007.

978 McMillan, H.: Linking hydrologic signatures to hydrologic processes: A Review, *Hydrol. Process.*, 34, 1393–1409,  
979 <https://doi.org/10.1002/hyp.13632>, 2020.

980 McMillan, H., Gueguen, M., Grimon, E., Woods, R., Clark, M., and Rupp, D. E.: Spatial variability of hydrological processes  
981 and model structure diagnostics in a 50 km<sup>2</sup> catchment, *Hydrol. Process.*, 28, 4896–4913, <https://doi.org/10.1002/hyp.9988>,  
982 2014.

983 McMillan, H., Westerberg, I., and Branger, F.: Five guidelines for selecting hydrological signatures, *Hydrol. Process.*, 31,  
984 4757–4761, <https://doi.org/10.1002/hyp.11300>, 2017.

985 McMillan, H., Araki, R., Bolotin, L., Kim, D.-H., Coxon, G., Clark, M., and Seibert, J.: Global patterns in observed hydrologic  
986 processes, *Nat Water*, <https://doi.org/10.1038/s44221-025-00407-w>, 2025.

987 McMillan, H. K.: A review of hydrologic signatures and their applications, *WIREs Water*, 8, <https://doi.org/10.1002/wat2.1499>,  
988 2021.

989 McMillan, H. K., Gnann, S. J., and Araki, R.: Large scale evaluation of relationships between hydrologic signatures and  
990 processes, *Water Resour. Res.*, 58, <https://doi.org/10.1029/2021wr031751>, 2022.

991 [McMillan, H., Coxon, G., Araki, R., Salwey, S., Kelleher, C., Zheng, Y., Knoben, W., Gnann, S., Seibert, J., and Bolotin, L.:](#)  
992 [When good signatures go bad: Applying hydrologic signatures in large sample studies, \*Hydrol. Process.\*, 37,](#)  
993 <https://doi.org/10.1002/hyp.14987>, 2023.

994 McMillan, H. K., Coxon, G., Araki, R., Salwey, S., Kelleher, C., Zheng, Y., Knoben, W., Gnann, S., Seibert, J., and Bolotin,  
995 L.: When good signatures go bad: Applying hydrologic signatures in large sample studies, *Hydrol. Process.*, 37,  
996 <https://doi.org/10.1002/hyp.14987>, 2023.

997 Miller, D. A. and White, R. A.: A conterminous United States multilayer soil characteristics dataset for regional climate and  
998 hydrology modeling, *Earth Interact.*, 2, 1–26, [https://doi.org/10.1175/1087-3562\(1998\)002<0001:acusms>2.3.co;2](https://doi.org/10.1175/1087-3562(1998)002<0001:acusms>2.3.co;2), 1998.

999 Miller, J. A.: Ground water atlas of the United States: Introduction and national summary (No. 730-A), A1–A15, 1999.

1000 Molnar, C., Bischl, B., and Casalicchio, G.: iml: An R package for Interpretable Machine Learning,  
1001 <https://doi.org/10.21105/joss.00786>, 2018.

1002 [Miller, D. A. and White, R. A.: A conterminous United States multilayer soil characteristics dataset for regional climate and](#)  
1003 [hydrology modeling, \*Earth Interact.\*, 2, 1–26, \[https://doi.org/10.1175/1087-3562\\(1998\\)002%3C0001:acusms%3E2.3.co;2\]\(https://doi.org/10.1175/1087-3562\(1998\)002%3C0001:acusms%3E2.3.co;2\),](#)  
1004 [1998.](#)

1005 Mosley, M. P.: Delimitation of New Zealand hydrologic regions, *J. Hydrol. (Amst.)*, 49, 173–192,  
1006 [https://doi.org/10.1016/0022-1694\(81\)90211-0](https://doi.org/10.1016/0022-1694(81)90211-0), 1981.

1007 Muñoz Sabater, J.: ERA5-Land monthly averaged data from 1950 to present, <https://doi.org/10.24381/CDS.68D2BB30>, 2019.

1008 Neff, B. P., Day, S. M., Piggott, A. R., and Fuller, L. M.: Base flow in the Great Lakes Basin,  
1009 <https://doi.org/10.3133/sir20055217>, 2005.

1010 Noguchi, S., Nik, A. R., Yusop, Z., Tani, M., and Sammori, T.: Rainfall-runoff responses and roles of soil moisture variations  
1011 to the response in tropical Rain Forest, Bukit Tarek, peninsular Malaysia, *J. Forest Res.*, 2, 125–132,  
1012 <https://doi.org/10.1007/bf02348209>, 1997.

1013 Ogden, F., Avant, B., Bartel, R., Blodgett, D., Clark, E., Coon, E., Cosgrove, B., Cui, S., Kindl da Cunha, L., Farthing, M.,  
1014 Flowers, T., Frame, J., Frazier, N., Graziano, T., Gutenson, J., Johnson, D., McDaniel, R., Moulton, J., Loney, D., Peckham,  
1015 S., Mattern, D., Jennings, K., Williamson, M., Savant, G., Tubbs, C., Garrett, J., Wood, A., and Johnson, J.: The Next  
1016 Generation Water Resources Modeling Framework: Open Source, Standards Based, Community Accessible, Model  
1017 Interoperability for Large Scale Water Prediction, AGU Fall Meeting Abstracts, New Orleans, LA, 2021, H43D–01, 2021.

1018 Omernik, J. M.: Ecoregions of the conterminous United States, *Ann. Assoc. Am. Geogr.*, 77, 118–125, 1987.

1019 Omernik, J. M.: Perspectives on the nature and definition of ecological regions, *Environ. Manage.*, 34 Suppl 1, S27–38,  
1020 <https://doi.org/10.1007/s00267-003-5197-2>, 2004.

1021 Oswald, C. J., Kelleher, C., Ledford, S. H., Hopkins, K. G., Sytsma, A., Tetzlaff, D., Toran, L., and Voter, C.: Integrating  
1022 urban water fluxes and moving beyond impervious surface cover: A review, *J. Hydrol. (Amst.)*, 618, 129188,  
1023 <https://doi.org/10.1016/j.jhydrol.2023.129188>, 2023.

1024 Oudin, L., Andréassian, V., Perrin, C., Michel, C., and Le Moine, N.: Spatial proximity, physical similarity, regression and  
1025 unged catchments: A comparison of regionalization approaches based on 913 French catchments, *Water Resources Research*,  
1026 44, <https://doi.org/10.1029/2007WR006240>, 2008.

1027 Paola, C., Fofoula-Georgiou, E., Dietrich, W. E., Hondzo, M., Mohrig, D., Parker, G., Power, M. E., Rodriguez-Iturbe, I.,  
1028 [Veldkamp, T. I. E., Wada, Y., Aerts, J. C. J. H., Döll, P., Gosling, S. N., Liu, J., Masaki, Y., Oki, T., Ostberg, S., Pokhrel, Y.,](#)  
1029 [Satoh, Y., Kim, H., and Ward, P. J.:](#) Water scarcity hotspots travel downstream due to human interventions in the 20th and  
1030 21st century, *Nat. Commun.*, 8, 15697, <https://doi.org/10.1038/ncomms15697>, 2017.

1031 [Vogel, R. M., Member, J., and Asce, N. M.:](#) Flow-duration curves. I: New interpretation and confidence intervals, [https://bpb-](https://bpb-us-e1.wpmucdn.com/sites.tufts.edu/dist/a/4406/files/2019/04/flowDuration1.pdf)  
1032 [us-e1.wpmucdn.com/sites.tufts.edu/dist/a/4406/files/2019/04/flowDuration1.pdf](https://bpb-us-e1.wpmucdn.com/sites.tufts.edu/dist/a/4406/files/2019/04/flowDuration1.pdf).

1033 Voller, V., and Wilcock, P.: Toward a unified science of the Earth's surface: Opportunities for synthesis among hydrology,  
1034 geomorphology, geochemistry, and ecology, *Water Resour. Res.*, 42, <https://doi.org/10.1029/2005wr004336>, 2006.

1035 [Payn, R. A., Gooseff, M. N., and McGlynn, B. L.:](#) Exploring changes in the spatial distribution of stream baseflow generation  
1036 during a seasonal recession, <https://doi.org/10.1029/2011WR011552>, 2012.

1037 Pechlivanidis, I. G. and Arheimer, B.: Large-scale hydrological modelling by using modified PUB recommendations: the  
1038 India-HYPE case, *Hydrol. Earth Syst. Sci.*, 19, 4559–4579, <https://doi.org/10.5194/hess-19-4559-2015>, 2015.

1039 Pedregosa, F., Varoquaux, G., Gramfort, A., Michel, V., Thirion, B., Grisel, O., Blondel, M., Prettenhofer, P., Weiss, R.,  
1040 Dubourg, V., Vanderplas, J., Passos, A., Cournapeau, D., Brucher, M., Perrot, M., and Duchesnay, E.: Scikit-learn: Machine  
1041 Learning in Python, *Journal of Machine Learning Research*, 12, 2825–2830, 2011.

1042 Penna, D.: A recipe for why and how to set up and sustain an experimental catchment, *Hydrol. Process.*, 38,  
1043 <https://doi.org/10.1002/hyp.15163>, 2024.

1044 Peters, N. E. and Aulenbach, B. T.: Water storage at the Panola mountain research watershed, Georgia, USA: Water storage  
1045 at pmrw, *Hydrol. Process.*, 25, 3878–3889, <https://doi.org/10.1002/hyp.8334>, 2011.

1046 Pfister, L., Martínez-Carreras, N., Hissler, C., Klaus, J., Carrer, G. E., Stewart, M. K., and McDonnell, J. J.: Bedrock geology  
1047 controls on catchment storage, mixing, and release: A comparative analysis of 16 nested catchments, *Hydrological Processes*,  
1048 31, 1828–1845, <https://doi.org/10.1002/hyp.11134>, 2017.

1049 Prieto, C., Kavetski, D., Le Vine, N., Álvarez, C., and Medina, R.: Identification of dominant hydrological mechanisms using  
1050 Bayesian inference, multiple statistical hypothesis testing, and flexible models, *Water Resour. Res.*, 57,  
1051 <https://doi.org/10.1029/2020wr028338>, 2021.

1052 Qi, S. L. and Mason, C. A.: Data used to prioritize the selection of river basins for intensive monitoring and assessment by the  
1053 U.S. Geological Survey, <https://doi.org/10.5066/P98194QR>, 2023.

1054 R Core Team (2024). R: A Language and Environment for Statistical Computing. R Foundation for Statistical Computing,  
1055 Vienna, Austria. <https://www.R-project.org/>.

1056 Reinecke, R., Stein, L., Gnann, S., Andersson, J. C. M., Arheimer, B., Bierkens, M., Bonetti, S., Güntner, Kollet, S., Mishra,  
1057 S., Moosdorf, N., Nazari, S., Pokhrel, Y., Prudhomme, C., Schewe, J., Shen, C., and Wagener, T.: Uncertainties guide global  
1058 water model advancement, *WIREs Water*, 12, <https://doi.org/10.1002/wat2.70025>, 2025.

1059 [Renken, R. A.: Ground Water Atlas of the United States: Segment 5. Arkansas, Louisiana, Mississippi. Hydrologic Atlas 730.](#)  
1060 [28p., U.S. Geological Survey, <https://doi.org/10.3133/ha730F>, 1998.](#)

1061 Robert Maier, H., Rosa Taghikhah, F., Nabavi, E., Razavi, S., Gupta, H., Wu, W., Radford, D. A. G., and Huang, J.: How  
1062 much X is in XAI: Responsible use of “Explainable” artificial intelligence in hydrology and water resources, *J. Hydrol.* X, 25,  
1063 100185, <https://doi.org/10.1016/j.hydroa.2024.100185>, 2024.

1064 [Rudlang, J. M., do Nascimento, T. V. M., van der Ent, R., Fenicia, F., and Hrachowitz, M.: Climate and landscape jointly](#)  
1065 [control Europe's hydrology. EGUsphere \[preprint\], <https://doi.org/10.5194/egusphere-2025-6372>, 2025.](#)

1066 Safeeq, M. and Hunsaker, C. T.: Characterizing runoff and water yield for headwater catchments in the southern Sierra Nevada,  
1067 *J. Am. Water Resour. Assoc.*, 52, 1327–1346, <https://doi.org/10.1111/1752-1688.12457>, 2016.

1068 Safeeq, M., Grant, G. E., Lewis, S. L., and Tague, C. L.: Coupling snowpack and groundwater dynamics to interpret historical  
1069 streamflow trends in the western United States: COUPLING SNOWPACK AND GROUNDWATER DYNAMICS TO  
1070 INTERPRET STREAMFLOW, *Hydrol. Process.*, 27, 655–668, <https://doi.org/10.1002/hyp.9628>, 2013.

1071 Santhi, C., Allen, P. M., Muttiah, R. S., Arnold, J. G., and Tuppard, P.: Regional estimation of base flow for the conterminous  
1072 United States by hydrologic landscape regions, *J. Hydrol. (Amst.)*, 351, 139–153,  
1073 <https://doi.org/10.1016/j.jhydrol.2007.12.018>, 2008.

1074 Sauquet, E., Shanafield, M., Hammond, J. C., Sefton, C., Leigh, C., and Detry, T.: Classification and trends in intermittent  
1075 river flow regimes in Australia, northwestern Europe and USA: A global perspective, *J. Hydrol. (Amst.)*, 597, 126170,  
1076 <https://doi.org/10.1016/j.jhydrol.2021.126170>, 2021.

1077 Seaber, P. R., Kapinos, F. P., and Knapp, G. L.: Hydrologic unit maps, US Geological Survey, <https://doi.org/10.3133/wsp2294>,  
1078 1987.

1079 Sebestyen, S. D., Shanley, J. B., Blume, T., Duncan, J. M., Jones, J., Segura, C., and Mast, M. A.: Introduction to the special  
1080 issue on research and observatory catchments, *Hydrol. Process.*, 39, <https://doi.org/10.1002/hyp.70069>, 2025.

1081 Shalev, G. and Kratzert, F.: Caravan MultiMet: Extending Caravan with multiple weather nowcasts and forecasts, arXiv  
1082 [cs.LG], arXiv, 2024.

1083 [Shanley, J. B., Sebestyen, S. D., McDonnell, J. J., McGlynn, B. L., and Dunne, T.: Water's Way at Sleepers River watershed](#)  
1084 [– revisiting flow generation in a post-glacial landscape, Vermont USA, \*Hydrol. Process.\*, 29, 3447–3459,](#)  
1085 <https://doi.org/10.1002/hyp.10377>, 2015.

1086 Shapley, L. S.: 17. A Value for n-Person Games, in: *Contributions to the Theory of Games (AM-28)*, Volume II, edited by:  
1087 Kuhn, H. W. and Tucker, A. W., Princeton University Press, Princeton, 307–318, <https://doi.org/10.1515/9781400881970-018>,  
1088 1953.

1089 Shaw, S. B. and Riha, S. J.: Examining individual recession events instead of a data cloud: Using a modified interpretation of  
1090  $dQ/dt-Q$  streamflow recession in glaciated watersheds to better inform models of low flow, *J. Hydrol. (Amst.)*, 434-435, 46–  
1091 54, <https://doi.org/10.1016/j.jhydrol.2012.02.034>, 2012.

1092 Shrestha, D., Howard, D., and Benedict, T. D.: Moderate Resolution Imaging Spectroradiometer (MODIS) irrigated  
1093 Agriculture datasets for the conterminous United States (MIRAD-US), <https://doi.org/10.5066/P9NA3EO8>, 2019.

1094 Sivapalan, M.: Pattern, process and function: Elements of a unified theory of hydrology at the catchment scale, in:  
1095 *Encyclopedia of Hydrological Sciences*, Wiley, Chichester, UK, <https://doi.org/10.1002/0470848944.hsa012>, 2005.

1096 Web Soil Survey: <http://websoilsurvey.nrcs.usda.gov/>, last access: 11 May 2025.

1097 Spieler, D., Mai, J., Craig, J. R., Tolson, B. A., and Schütze, N.: Automatic model structure identification for conceptual  
1098 hydrologic models, *Water Resour. Res.*, 56, <https://doi.org/10.1029/2019wr027009>, 2020.

1099 [Stein, L., Clark, M. P., Knoben, W. J., Pianosi, F., & Woods, R. A.: How do climate and catchment attributes influence flood  
1100 generating processes? A large-sample study for 671 catchments across the contiguous USA. \*Water Resources Research\*, 57\(4\),  
1101 e2020WR028300. <https://doi.org/10.1029/2020WR028300>, 2021.](#)

1102 Stets, E. G., Archer, A. A., Degnan, J. R., Erickson, M. L., Gorski, G., Medalie, L., and Scholl, M. A.: The National integrated  
1103 water availability assessment, 2025.

1104 Tague, C. and Grant, G. E.: A geological framework for interpreting the low-flow regimes of Cascade streams, Willamette  
1105 River Basin, Oregon: GEOLOGICAL FRAMEWORK FOR LOW-FLOW REGIMES, *Water Resour. Res.*, 40,  
1106 <https://doi.org/10.1029/2003wr002629>, 2004.

1107 Tague, C. and Grant, G. E.: Groundwater dynamics mediate low-flow response to climate warming in snow-dominated alpine  
1108 regions, *Water Resources Research*, 45, 2009.

1109 Tallaksen, L. M.: A review of baseflow recession analysis, *J. Hydrol.*, 165, 349–370, [https://doi.org/10.1016/0022-  
1110 1694\(94\)02540-R](https://doi.org/10.1016/0022-1694(94)02540-R), 1995.

1111 Tarasova, L., Gnann, S., Yang, S., Hartmann, A., and Wagener, T.: Catchment characterization: Current descriptors,  
1112 knowledge gaps and future opportunities, *Earth Sci. Rev.*, 252, 104739, <https://doi.org/10.1016/j.earscirev.2024.104739>, 2023.

1113 Thompson, J. M., Hathaway, J. M., Perfect, E., and Schwartz, J. S.: The effect of stormwater infiltration and surrounding built  
1114 infrastructure on local groundwater dynamics: a case study for regenerative stormwater conveyances, *Sustain. Resilient  
1115 Infrastruct.*, 1–11, <https://doi.org/10.1080/23789689.2020.1772636>, 2020.

1116 Trancoso, R., Phinn, S., McVicar, T., Larsen, J., and McAlpine, C.: Regional variation in streamflow drivers across a  
1117 continental climatic gradient, *Ecohydrology*, 10, e1816, <https://doi.org/10.1002/eco.1816>, 2017.

1118 Tran, V. N.: CAMELSH: A large-sample hourly hydrometeorological dataset and attributes at watershed-scale for contiguous  
1119 United States, <https://doi.org/10.5281/ZENODO.15070091>, 2025.

1120 Tran, V. N., Xu, D., Van Nguyen, T., Kim, T., and Ivanov, V. Y.: CAMELSH: A large-sample hourly hydrometeorological  
1121 dataset and attributes at watershed-scale for CONUS, *Sci. Data*, 12, 1307, <https://doi.org/10.1038/s41597-025-05612-6>, 2025.

1122 Turner, S., Hannaford, J., Barker, L. J., Suman, G., Killeen, A., Armitage, R., Chan, W., Davies, H., Griffin, A., Kumar, A.,  
1123 Dixon, H., Albuquerque, M. T. D., Almeida Ribeiro, N., Alvarez-Garreton, C., Amoussou, E., Arheimer, B., Asano, Y.,  
1124 Berezowski, T., Bodian, A., Boutaghane, H., Capell, R., Dakhaoui, H., Daňhelka, J., Do, H. X., Ekkawatpanit, C., El Khalki,  
1125 E. M., Fleig, A. K., Fonseca, R., Giraldo-Osorio, J. D., Goula, A. B. T., Hanel, M., Horton, S., Kan, C., Kingston, D. G., Laaha,  
1126 G., Laugesen, R., Lopes, W., Mager, S., Rachdane, M., Markonis, Y., Medeiro, L., Midgley, G., Murphy, C., O'Connor, P.,  
1127 Pedersen, A. I., Pham, H. T., Piniewski, M., Renard, B., Saidi, M. E., Schmockler-Fackel, P., Stahl, K., Thyer, M., Toucher,  
1128 M., Trambly, Y., Uusikivi, J., Venegas-Cordero, N., Visessri, S., Watson, A., Westra, S., and Whitfield, P. H.: ROBIN:  
1129 Reference observatory of basins for international hydrological climate change detection, *Sci. Data*, 12, 654,  
1130 <https://doi.org/10.1038/s41597-025-04907-y>, 2025.

1131 UKIH: UK Institute of Hydrology (Great Britain), Low Flow Studies Reports, Institute of Hydrology, 1980.

1132 United States Department of Agriculture, Soil Survey Staff, and Natural Resources Conservation: U.S. General Soil Map  
1133 (STATSGO): Web soil survey, 2008.

1134 United States Geological Survey: Protected Areas Database of the United States (PAD-US) 4,  
1135 <https://doi.org/10.5066/P96WBCHS>, 2024.

1136 U.S. Environmental Protection Agency: National Hydrography Dataset Plus (NHDPlus): USEPA; USGS; and Horizon  
1137 Systems Corporation, 2008.

1138 U.S. Geological Survey: USGS Water Data for the Nation: U.S. Geological Survey National Water Information System  
1139 Database, <https://doi.org/10.5066/F7P55KJN>, 2025.

1140 Valeron, B. and Meixner, T.: Overland flow generation in chaparral ecosystems: temporal and spatial variability, *Hydrol.*  
1141 *Process.*, 24, 65–75, <https://doi.org/10.1002/hyp.7455>, 2010.

1142 Van Metre, P. C., Qi, S., Deacon, J., Dieter, C., Driscoll, J. M., Fienen, M., Kenney, T., Lambert, P., Lesmes, D., Mason, C.  
1143 A., Mueller-Solger, A., Musgrove, M., Painter, J., Rosenberry, D., Sprague, L., Tesoriero, A. J., Windham-Myers, L., and  
1144 Wolock, D.: Prioritizing river basins for intensive monitoring and assessment by the US Geological Survey, *Environ. Monit.*  
1145 *Assess.*, 192, 458, <https://doi.org/10.1007/s10661-020-08403-1>, 2020.

1146 Westerberg, I. K., Wagener, T., Coxon, G., McMillan, H. K., Castellarin, A., Montanari, A., and Freer, J.: Uncertainty in  
1147 hydrological signatures for gauged and ungauged catchments, *Water Resources Research*, 52, 1847–1865,  
1148 <https://doi.org/10.1002/2015WR017635>, 2016.

1149 Wiczorek, M. E. and LaMotte, A. E.: Attributes for NHDPlus Catchments (Version 1.1) for the Conterminous United States:  
1150 Average Saturation Excess-Overland Flow, 2002: U.S. Geological Survey data release, 2010.

1151 Wiczorek, M. E., Hafen, K. C., and Staub, L. E.: Data-Driven Drought Prediction Project model inputs for Upper and Lower  
1152 Colorado portions of the national hydrologic Geo-spatial fabric version 1.1 and select U.S. geological Survey streamgage basins  
1153 (ver. 2.0, July 2025), <https://doi.org/10.5066/P98IG8LO>, 2023.

1154 Willard, J. D., Ciulla, F., Weierbach, H., Kumar, V., and Varadarajan, C.: Evaluating deep learning approaches for predictions  
1155 in unmonitored basins with continental-scale stream temperature models, *arXiv [cs.LG]*, arXiv, 2024.

1156 Williams, P. W. and Ford, D. C.: Global distribution of carbonate rocks, *Zeitschrift für Geomorphologie Suppl.*, 147, 1–2, 2006.

1157 Wilson, C. G., Papanicolaou, A. N. T., and Denn, K. D.: Partitioning fine sediment loads in a headwater system with intensive  
1158 agriculture, *J. Soils Sediments*, 12, 966–981, <https://doi.org/10.1007/s11368-012-0504-2>, 2012.

1159 Winter, T. C.: The Concept of Hydrologic Landscapes, *JAWRA Journal of the American Water Resources Association*, 37,  
1160 335–349, <https://doi.org/10.1111/j.1752-1688.2001.tb00973.x>, 2001.

1161 Wlostowski, A. N., Molotch, N., Anderson, S. P., Brantley, S. L., Chorover, J., Dralle, D., Kumar, P., Li, L., Lohse, K. A.,  
1162 Mallard, J. M., McIntosh, J. C., Murphy, S. F., Parrish, E., Safeeq, M., Seyfried, M., Shi, Y., and Harman, C.: Signatures of  
1163 Hydrologic Function Across the Critical Zone Observatory Network, *Water Resour. Res.*, 57, e2019WR026635,  
1164 <https://doi.org/10.1029/2019wr026635>, 2021.

1165 Wolock, D. M.: Hydrologic landscape regions of the United States, US Geological Service, 2003a.

1166 Wolock, D. M.: Infiltration-excess overland flow estimated by TOPMODEL for the conterminous United States (No. 2003-  
1167 310), US Geological Survey., 2003b.

1168 Wu, S., Zhao, J., Wang, H., and Sivapalan, M.: Regional patterns and physical controls of streamflow generation across the  
1169 conterminous United States, *Water Resour. Res.*, 57, e2020WR028086, <https://doi.org/10.1029/2020wr028086>, 2021.

1170 Xia, Y., Mitchell, K., Ek, M., Sheffield, J., Cosgrove, B., Wood, E., Luo, L., Alonge, C., Wei, H., Meng, J., Livneh, B.,  
1171 Lettenmaier, D., Koren, V., Duan, Q., Mo, K., Fan, Y., and Mocko, D.: Continental-scale water and energy flux analysis and  
1172 validation for the North American Land Data Assimilation System project phase 2 (NLDAS-2): 1. Intercomparison and  
1173 application of model products, *J. Geophys. Res. D: Atmos.*, 117, <https://doi.org/10.1029/2011JD016048>, 2012.

1174 Xie, J., Liu, X., Jasechko, S., Berghuijs, W. R., Wang, K., Liu, C., Reichstein, M., Jung, M., and Koirala, S.: Majority of global  
1175 river flow sustained by groundwater, *Nat. Geosci.*, 17, 770–777, <https://doi.org/10.1038/s41561-024-01483-5>, 2024.

1176 Yang, L., Jin, S., Danielson, P., Homer, C., Gass, L., Bender, S. M., Case, A., Costello, C., Dewitz, J., Fry, J., Funk, M.,  
1177 Granneman, B., Liknes, G. C., Rigge, M., and Xian, G.: A new generation of the United States National Land Cover Database:  
1178 Requirements, research priorities, design, and implementation strategies, *ISPRS J. Photogramm. Remote Sens.*, 146, 108–123,  
1179 <https://doi.org/10.1016/j.isprsjprs.2018.09.006>, 2018.

1180 Yilmaz, K. K., Gupta, H. V., and Wagener, T.: A process-based diagnostic approach to model evaluation: Application to the  
1181 NWS distributed hydrologic model, *Water Resour. Res.*, 44, <https://doi.org/10.1029/2007wr006716>, 2008.

1182 Zimmer, M. A. and Gannon, J. P.: Run-off processes from mountains to foothills: The role of soil stratigraphy and structure  
1183 in influencing run-off characteristics across high to low relief landscapes, *Hydrol. Process.*, 32, 1546–1560,  
1184 <https://doi.org/10.1002/hyp.11488>, 2018.

1185 Zipper, S. C., Hammond, J. C., Shanafeld, M., Zimmer, M., Detry, T., Jones, C. N., Kaiser, K. E., Godsey, S. E., Burrows, R.  
1186 M., Blaszcak, J. R., Busch, M. H., Price, A. N., Boersma, K. S., Ward, A. S., Costigan, K., Allen, G. H., Krabbenhoft, C. A.,  
1187 Dodds, W. K., Mims, M. C., Olden, J. D., Kampf, S. K., Burgin, A. J., and Allen, D. C.: Pervasive changes in stream  
1188 intermittency across the United States, *Environ. Res. Lett.*, 16, 084033, <https://doi.org/10.1088/1748-9326/ac14ec>, 2021.